

# Characterizing the Galactic and Extragalactic Background Near Exoplanet Direct Imaging Targets

Authors: M. Cracraft<sup>1</sup>, R. J. De Rosa<sup>2</sup>, W. Sparks<sup>3</sup>, V. P. Bailey<sup>4</sup>, M. Turnbull<sup>5</sup>

**Abstract:** As more missions attempt to directly image and characterize exoplanets orbiting nearby sun-like stars, advance characterization of possible contaminating background sources becomes more important and can impact target selection. This paper describes an exploration of the Hubble Source catalog, Gaia catalog and Besançon galaxy simulations in order to determine the likelihood of having a contaminating source in the background of a set of high proper motion stars in the expected timeframe of observations for the Nancy Grace Roman Space Telescope Coronagraphic Instrument. The analysis shows that for most of the targets, there is a very low possibility of a star falling within the CGI field of view, but that at low galactic latitudes where there is a greater density of sources, faint stellar background sources could be a concern.

## 1. Introduction

There is a growing impetus for spaceborne missions to directly image and characterize Earth-sized and larger exoplanets orbiting nearby sunlike stars. Advance characterization of confounding background sources in near-future planet hunting fields has the potential to critically impact target selection and observing strategy of these missions. Here, we describe such a project motivated by potential observing programs to use the Nancy Grace Roman Space Telescope (Roman) Coronagraphic Instrument (CGI), but with broad application to other telescopes and missions.

Since astrophysical background sources may be confused with exoplanets orbiting target stars, and hence hamper our ability to identify and characterize such exoplanets, we sought to determine both empirically and statistically the likelihood of encountering background “contaminating” sources. To do this, we extracted images from the Hubble Space Telescope (HST) archives of regions close to target stars which had been observed by HST in order to empirically check for any nearby potentially contaminating stars, galaxies or other astrophysical sources near the target stars, projected forward to the era of the Roman observations. We also examine the Gaia DR2 catalog to determine (a) whether any identified Gaia stars would be near enough to interfere with Roman CGI observations and (b) compare the Gaia catalog to a set of Besançon galaxy simulated catalogs to determine how well that statistical model reproduced the empirical Gaia catalogs at the explicit pointings represented by the CGI targets, and hence tie the empirical likelihood of contamination to a more widely applicable statistical approach.

CGI will observe both exoplanets and circumstellar disks during its technology demonstration phase. As the highest priority circumstellar disk targets (eg: HR 4796), and self-luminous exoplanet targets (eg: HR 8799), already have deep adaptive optics imaging that can be used to identify background contaminants, we concentrate here instead on the potential reflected-light exoplanet targets (Table 1). These targets all host known exoplanets, which were detected by radial velocity (RV) but have not yet been directly imaged.

1) Space Telescope Science Institute, 3700 San Martin Drive, Baltimore MD 21218

2) European Southern Observatory, Alonso de Córdova 3107, Vitacura, Santiago, Chile

3) Space Telescope Science Institute (Emeritus) and SETI Institute

4) Jet Propulsion Laboratory, California Institute of Technology, 4800 Oak Grove Dr, Pasadena CA, 91109

5) SETI Institute 189 Bernardo Ave, Suite 200. Mountain View, CA 94043, United States

*Table 1* Properties of potential CGI targets: J2000 coordinates in RA and Dec, Galactic Latitude and Longitude and proper motions; Parallax, Proper Motion in RA and Dec (mas/yr). These systems host known radial velocity-detected planets, some of which might be detectable with CGI. All coordinates listed were taken from SIMBAD. The last column indicates whether we have Hubble data for each target.

Target	RA (h:m:s)	Dec (d:m:s)	Gal. Lat (deg)	Gal. Long. (deg)	Parallax (mas)	PM RA (mas/yr)	PM Dec (mas/yr)	HST
14 Her	16 10 24.315	+43 49 03.499	46.94	69.17	55.74	132.02	-296.46	
47 Uma	10 59 27.974	+40 25 48.922	63.37	175.78	72.45	-317.64	55.01	
55 Cnc	08 52 35.811	+28 19 50.957	37.70	196.79	79.43	-485.87	-233.65	yes
ε Eri	03 32 55.845	-09 27 29.731	-48.05	195.84	310.94	-975.17	19.49	yes
HD 142	00 06 19.175	-49 04 30.682	-66.39	321.59	38.89	575.29	-39.19	
HD 39091	05 37 09.885	-80 28 08.831	-29.78	292.51	54.71	311.19	1048.85	
HD 114613	13 12 03.183	-37 48 10.879	24.89	307.42	49.27	-381.63	46.09	
HD 134987	15 13 28.667	-25 18 33.655	27.39	339.19	38.17	-400.31	-75.16	
HD 154345	17 02 36.404	+47 04 54.763	37.66	73.02	54.66	123.20	853.74	
HD 160691	17 44 08.704	-51 50 02.591	-11.49	340.06	64.08	-15.31	190.92	
HD 190360	20 03 37.405	+29 53 48.495	-0.67	67.41	62.44	683.34	-525.68	
HD 192310	20 15 17.392	-27 01 58.714	-29.40	15.62	113.65	1242.53	-181.04	
HD 217107	22 58 15.541	-02 23 43.387	-53.32	70.47	49.82	-7.11	-14.78	
HD 219134	23 13 16.975	+57 10 06.0765	-3.20	109.90	153.08	2074.52	294.94	
τ Ceti	01 44 04.083	-15 56 14.927	-73.44	173.10	273.96	-1721.05	854.16	yes
υ And	01 36 47.842	+41 24 19.644	-20.67	132.00	74.12	-173.33	-381.8	yes

## 2. Observational and Statistical Approach

In order to determine the likelihood of background contamination of CGI observations empirically, a variety of catalogs and archived images were used to examine the background regions of the selected targets.

We checked whether there is any background source within the field of view of the target star at the time when the observations would likely be taken. For this document, the year 2026 is the assumed launch date and fall of 2026 is the likely date of observation. There are several regions to be considered for the CGI instrument.

The high-contrast region for the primary observing mode (Band 1 with the Hybrid Lyot Coronagraph) has a diameter of 0.9 arcseconds (575 nm with outer working angle  $\lambda/D = 9$ ). The high-contrast region for the secondary imaging mode Band 4 with the Shaped Pupil “Wide” FOV Coronagraph has diameter 2.9 arcseconds (imaging at 825 nm with  $\lambda/D = 20$ ). The flux ratio

detection limit in these observing modes is  $10^{-8} - 10^{-9}$ . The non-coronagraphic field of view has diameter 7.2 arcseconds, but high-contrast observations cannot be taken in non-coronagraphic mode. Hence, the coronagraphic field of view is the most important region to be clear of background sources as well as ‘glints’ from nearby objects. No stars of equal brightness to the target star may be present within about 45” of the target, with increasingly stringent limits at smaller separations: nothing  $\sim$ 5-7 magnitudes fainter within 10” of the region of interest, nothing  $\sim$ 15 magnitudes fainter within 2” of the region of interest.

Initially we examined the Hubble Source Catalog (HSC) and Hubble Legacy Archive (HLA) to see if there were images available covering the positions of the targets in current times as well as dates in 2026, taking into account the expected proper motion of the target stars. Since there was only Hubble data currently existing for a few targets, as listed in Table 1, the Gaia DR2 catalog was examined for the full target list. The Gaia catalogs provide empirical relatively uniform statistics on the number and density of sources near the targets, whereas even where Hubble data exists, it is heterogeneous. The Hubble Source Catalog is derived from all existing observations, from a variety of observing programs, utilizing different instruments, filters and exposure times, making for an inhomogeneous data set. By combining information from both Gaia and HST (where available), a better understanding of the expected characteristics of the background of the target stars and nearby regions can be obtained. The Besançon statistical model for Galaxy star count simulations was also examined, to compare the predicted star counts at different galactic latitudes to the observed values found with Gaia. The comparison between Gaia and Besançon allows us to use the Besançon simulations to extrapolate into fainter magnitudes than are found in the Gaia catalogs. The section below describes an in-depth exploration of the region of sky near Upsilon Andromeda ( $\nu$  And), one of the few sources that was well covered in both the HSC and Gaia, to illustrate our methods.

### 3. A case study: exploration of Upsilon Andromeda

This exploration started by examining the Mikulski Archive for Space Telescopes (MAST) contents for Hubble data on the target. By calculating the position of  $\nu$  And in 2026 taking into account the proper motion, it can be determined whether there is usable data covering the 2026 position and hence revealing the (future) background of the target star. The image below, Figure 1, shows a MAST image (DSS background) with a red cross-hair in the middle of the star image, with coordinates that match the J2000 coordinates on January 1, 2000, and second red cross-hair to the lower right marking the January 1, 2026 coordinates. The search for Hubble data for direct background observations should focus on the position calculated in 2026. As a double-check on the calculated 2026 position, the Gaia data was overplotted on the MAST DSS image. Since the Gaia DR2 data have a timeframe of approximately July of 2015, it should show consistent motion between the 2000 and 2026 dates. The pink square in the middle is a Gaia point source Gaia DR2 348020448377061376, which maps to  $\nu$  And in the Gaia timeframe. This does show consistent motion and is a good check on the calculations of the 2026 position. While there is a STIS image centered on  $\nu$  And taken in 2011, the future position (2026) is beyond the edge of any image currently existing in the Hubble data sets.

Table 2 Positions of Upsilon Andromeda in 2000 and 2026. The J2000 position and proper motion were found in SIMBAD and calculated out to the year 2026 in J2000 coordinates.

Coordinate	2000 Position	Proper Motion (mas/yr)	2026 position
RA	1:36:47.842	-173.33	1:36:47.442
Dec	+41:24:19.644	-381.8	+41:24:09.72



Figure 1 Current and future positions of  $\nu$  And on a DSS background. The red cross in the middle of the image marks the 2000 (January 1) coordinates, while the red cross to the lower right mark the 2026 coordinates. The pink box in between marks the Gaia position from July 2015. This shows the movement of the star over 26 years. The star to the right (pink box to the far right) is a potential contaminating star in the Gaia catalog

Where Hubble data exist, the MAST archive shows the footprint of all observations near or on the target, and allows a user to narrow down which data to examine by instrument and filter amongst other parameters. The approach taken here was to find several images in the field of interest that had consistent cameras and filters that gave large enough regions to allow for some statistical analysis and comparisons to the Gaia data set. For  $\nu$  And, there exists a set of three separated regions taken with the ACS camera, F775W filter that have a catalog of stars in the HSC.

These image footprints are shown in Figure 2. The footprints outlined in orange show where images are available in the HLA, while the red dots indicate the identified ACS/F775W HSC sources. The circle around the central target has a radius of 18 arcminutes. These three fields of view had processed images in the HLA. These fields combined 15 exposures, 31 exposures, and 30 exposures, for total exposure times of 9391, 16797 and 16302 seconds respectively. Combined images of this depth have very few remaining image artifacts such as cosmic rays. With all three images combined the resulting catalog extracted from the HSC contains over 2300 sources. The

catalog can be filtered to include only those sources identified in multiple images in order to exclude possible remaining spurious sources. This process results in approximately 50 sources brighter than 25<sup>th</sup> magnitude in F775W detected per square arcminute in these combined regions.

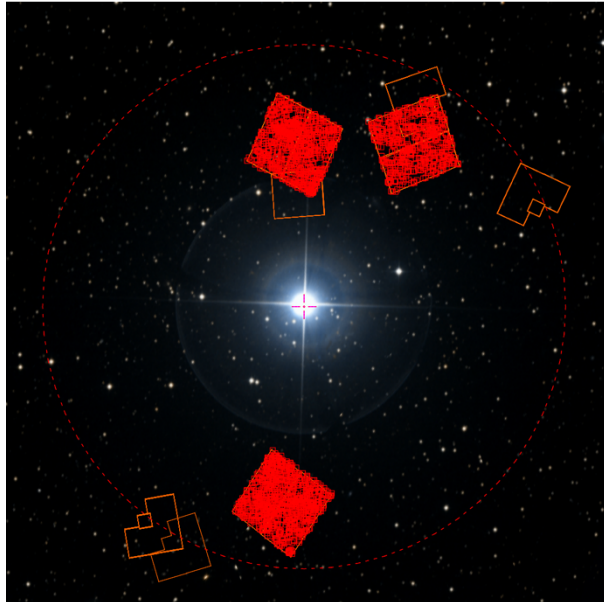


Figure 2 Footprint of  $\nu$  And Hubble data in the HLA, with the ACS/F775W HSC sources shown in red. The open wedge shapes are the outline of WFPC2 images. The circle to look for sources has an 18 arcminute radius.

Using the data found in the Hubble source catalog, we can plot a histogram of the sources found in the ACS F775W image set.

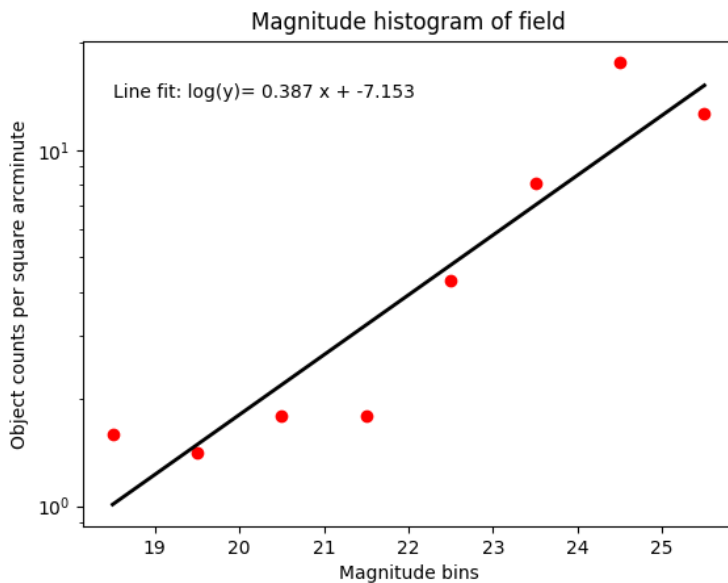


Figure 3 Histogram of the ACS F77W data from the Hubble source catalog. Y axis is number of sources found per square arcminute.

This is useful information from Hubble data, but as can be seen in Table 1, very few of the targets chosen actually have such extensive Hubble data. The Gaia DR2 offers a complementary catalog to the HSC, albeit to a depth much less than typical HST imaging. Gaia is complete to approximately 20 magnitudes while HST finds sources to magnitude 24 - 25. The advantage of Gaia DR2 is that it provides a consistent, relatively uniform, empirical dataset for all targets. All of the data was taken in the same manner and with the same filters. In order to determine stellar densities near the targets and thus the likelihood of having a contaminating source in a given observation, the Gaia DR2 release was therefore used to examine the background area of the targets in a 0.3 degree radius area centered on a target star.

With the Gaia data, color magnitude diagrams can be created for those regions using the different Gaia passbands, G (green), GBP (blue) and GRP (red) as shown here:

<https://www.cosmos.esa.int/web/gaia/iow 20180316>. An example of this color magnitude diagram is shown in Figure 4.

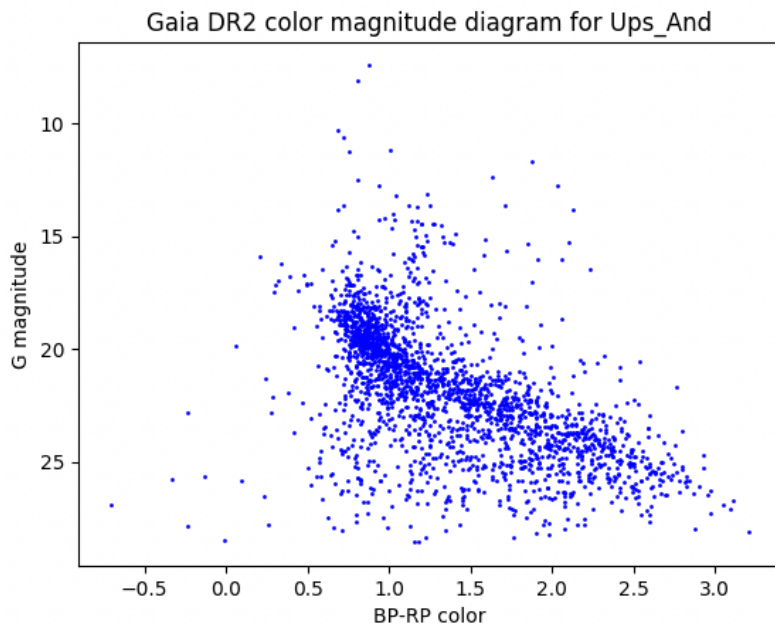


Figure 4 Color Magnitude Diagram for *v* And in Gaia magnitudes

We also created Besançon simulated catalogs for the target pointings to (a) compare the expected (model) stellar populations to actual data found with Gaia and the Hubble source catalog and (b) extrapolate the derived number density statistics to faint magnitude levels, consistent with anticipated exoplanet brightnesses. The simulations were run with mostly default settings, with the size of the region chosen to ensure  $\sim 100,000$  stars in each simulation and hence negligible Poisson counting uncertainties. (The models for positions near the galactic center therefore covered a smaller area than those with less densely populated areas at higher galactic latitude.) The magnitude and color limits were changed to include stars at all distances and run with a large

distance limit of 125kpc to encompass all possible stars. It is also worth noting that the Besançon model also includes a white dwarf and a brown dwarf component.

The number of Gaia sources in each magnitude bin can be plotted and compared to counts expected from the Besançon model to see how closely the models fit the empirical Gaia observations. To convert Besançon Vmag and colors to match the Gaia Gmag values, the following equation, as found in Gaia documentation, was used.

$$G = V - 0.0257 - 0.0924 \cdot (V-I) - 0.1623 \cdot (V-I)^2 + 0.0090 \cdot (V-I)^3$$

The Besançon model naturally covers a much wider magnitude range than can be observed with Gaia. The Gaia catalog has a magnitude limit of around G mag = 20, while the Besançon model goes to about a magnitude limit of 40, far fainter than required for the present purposes. If the comparison is limited to those regions with overlapping magnitude scales, from approximately 15 to 20, a direct comparison can be shown between the two, as seen in Figure 5.

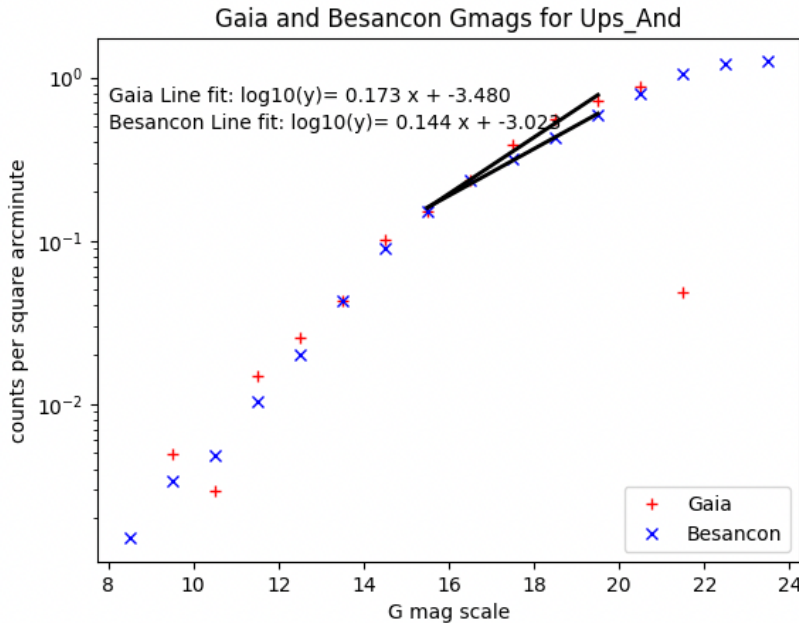


Figure 5 Gaia counts per magnitude bin per square arcminute compared to Besançon simulations of the same for *v And*.

It is also possible to combine the HSC histogram data of Figure 3 with the Gaia and Besançon catalogs. Since the Hubble data was taken in a redder filter than the Gaia G mag, the Hubble AB magnitudes were plotted against the Gaia magnitudes and an offset was found between them. In order to convert from ACS F775W magnitudes to Gaia G, an offset of 0.15 was added.

$$\text{Gmag} = \text{ACSmag} + 0.15$$

When this is done, it can be seen that there is an excess of sources at the faint end of the scale, around 24 magnitudes and higher. To obtain a grasp on the relative contribution of stars and galaxies (which are not well represented in the Gaia data and are not included in the Besançon model), the concentration index (CI) of the sources listed in the HSC can be used as a filter. This concentration index is defined as the difference in aperture magnitudes using a small and large aperture around the source. The rounder, more point-source-like objects have CI values closer to 1, while more extended sources tend to have higher CI value. Hence, by sorting out the ACS data and plotting the two groups separately, it can be seen that (a) the star like objects are in very good agreement with the Gaia catalog and the Besançon model, and (b) the faint source excess counts seen in the HSC data are very likely due to the emergence of a population of extragalactic sources, recognized by more their more extended CI parameterization, as shown in Figure 6. There were also instances seen in the data where the HSC identified multiple sources on a single target, like a spiral galaxy. Filtering the dataset as described above was an attempt to reject spurious hits, but some may remain in the final catalog, possibly artificially inflating the extended source counts.

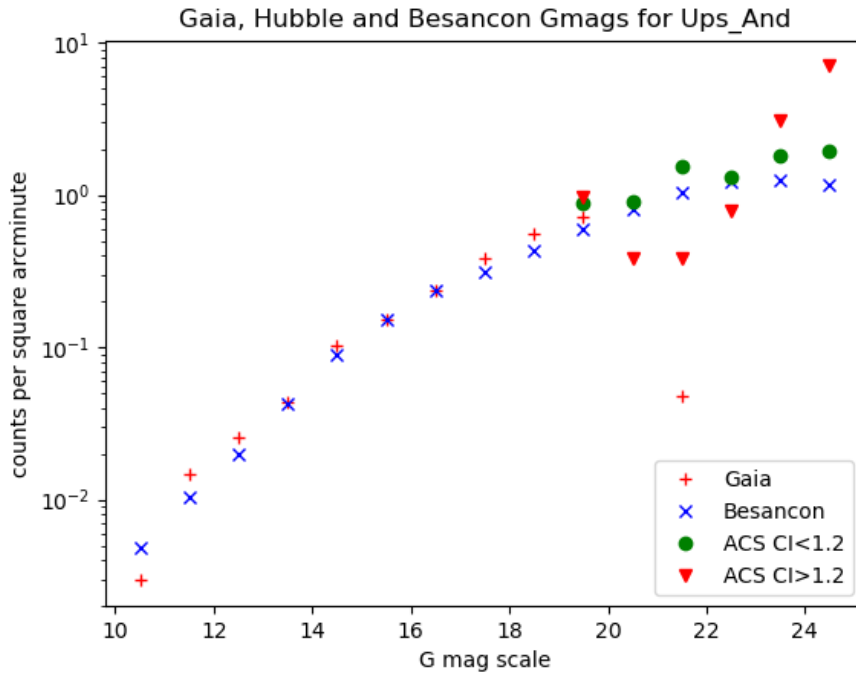


Figure 6 Comparison of Gaia, ACS and Besançon source counts per magnitudes per square arcminute near Upsilon Andromeda. The ACS data is separated out into point sources ( $CI < 1.2$ ) and extended sources ( $CI \geq 1.2$ )

Returning to the specifics of the individual stars near  $\nu$  And, by using the data in the Gaia catalog (current position and proper motion for all Gaia stars), the 2026 positions of the stars can be examined to determine which stars may be near to the target object in the desired timeframe, as also shown in Figure 1. For this example, the January 1, 2026 position of  $\nu$  And, as calculated from the SIMBAD J2000 coordinates, is determined to be: 01h 36m 47.4416s +41° 24' 09.7175". The list of stars within one arcminute of that position and their magnitudes as shown in the Gaia DR2 catalog are given in Table 3. The Gaia DR2 observations were in J2015.5 positions, so when the positions were calculated for the year 2026, this put the positions as they would be on July 2,

2026, creating a six-month difference to the SIMBAD position. The star with magnitude 3.89 is  $\nu$  And with position appropriate to July 2026. This can be seen more clearly in Figure 7. The red plus is the January 1, 2000 position and the red circle is the January 1, 2026 position of  $\nu$  And. The green  $\times$  on top of the red circle is from the Gaia catalog calculations of the position, July 2, 2026. The distance calculated in the table below is the distance of the Gaia field star positions from the target star in 2026. (The small difference in calculated positions between Gaia and SIMBAD coordinates, which are about six months apart, result in the distance for the target star not being 0, and could be indicative of the uncertainties in the proper motion calculations as well as the differing dates.)

Table 3 Positions of stars near Upsilon Andromeda in July 2026.. Position of  $\nu$  And highlighted in bold italics.. All positions listed are of stars in 2026, based on Gaia positions and proper motions.

Source ID	Distance (arcsec)	RA	Dec	G magnitude
348020242217448576	55.7656	01h36m49.9991s	+41d23m21.9506s	12.51
<b>348020448377061376</b>	<b>0.2047</b>	<b>01h36m47.4364s</b>	<b>+41d24m09.5213s</b>	<b>3.899</b>
348020448375872768	30.1985	01h36m44.9375s	+41d24m20.5898s	14.891
348020448375877632	36.9352	01h36m45.1585s	+41d23m43.1797s	16.142
348020448377062528	36.7454	01h36m45.1633s	+41d23m43.3916s	15.292

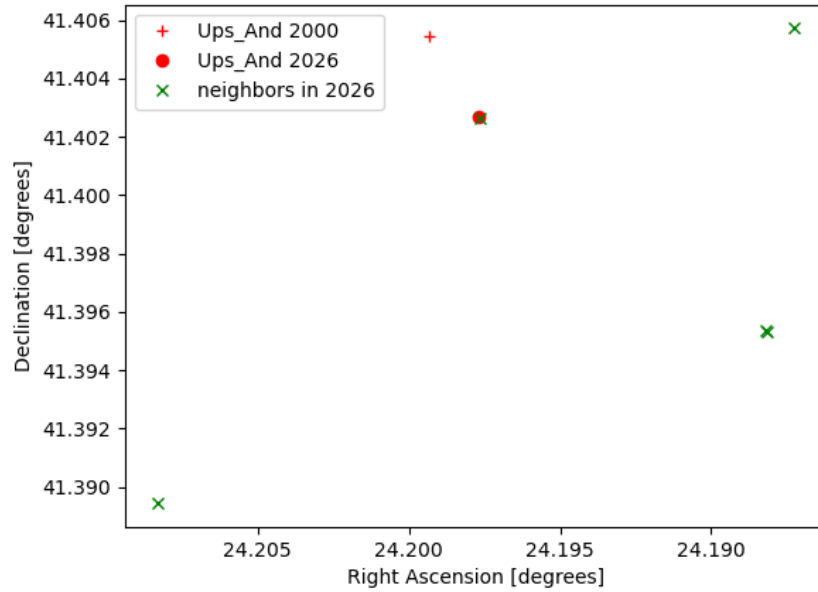


Figure 7 Position of  $\nu$  And in 2000 and 2026 with nearby neighbors at 2026 Gaia positions.

Conclusion for this case study: After examining the area around  $\nu$  And in Hubble imaging, the Gaia catalog and using the Besançon model, it appears very unlikely that there would be a background object within the CGI apertures that would interfere with any observations. Gaia shows no other catalogued source within the CGI FOV radius ( $\sim 7.2$  arcseconds) of the target source.

The widest coronagraphic FOV for Roman CGI is 2.9 arcseconds in diameter, so the two regions we will examine have areas of 6.61 and 40.72 squared arcseconds corresponding to the widest coronagraph FOV and the entire imaged field of view of the CGI.

The equations found by least-square fitting of a straight line to the Gaia data between magnitudes 15 and 20 where the best coverage exists can be used to estimate how many sources might be expected per square arcminute at specific desired magnitudes. (Equations are included within Figure 5 for  $\nu$  And; similar plots given in the appendices for each target star provide the slopes and intercepts for Table 5.)

Table 5 shows the predicted densities for all targets including  $\nu$  And in Gaia G mags for magnitude 20 and 24. These magnitudes are approximately 1 and 5 sources per square arcminute, respectively. These values give predicted densities for the apertures ranging from  $1.8 \times 10^{-3}$  to  $1.1 \times 10^{-2}$  stars in the regions of interest on the low end to  $19.2 \times 10^{-3}$  to  $5.6 \times 10^{-2}$  stars in the small and large areas of interest on the high end. This shows that there is a very low chance of a source brighter than Gmag of 24 falling by chance within the apertures. The expected probability of ‘glints’ due to brighter stars outside the field of view is also small, because the number density decreases with increasing star brightness.

#### 4. Statistical Analysis across the target set

By using the methods described for the case study above ( $\nu$  And) for the sample exploration, similar analysis can be applied to the rest of the dataset. While there is no HSC data for most targets, all targets have data from Gaia and the Besançon model. To compare the Gaia catalog and the Besançon model we obtain a ratio of counts per square arcminute in the overlapping magnitude bins, as shown in Figure 8 for  $\nu$  And. An average of the ratios between magnitude bins of 15 to 20 can be used as an approximation of how closely the Besançon model matches the observed counts in the Gaia DR2 catalog as shown Table 4 for all targets. The closer this ratio is to 1.0, the closer the Besançon model matches the Gaia catalog. Figure 9 shows this ratio plotted against galactic latitude to demonstrate that Gaia and the Besançon model are in close agreement except at latitudes near zero where small-spatial-scale variability in both extinction and stellar counts may not be well-captured in the Besançon model.

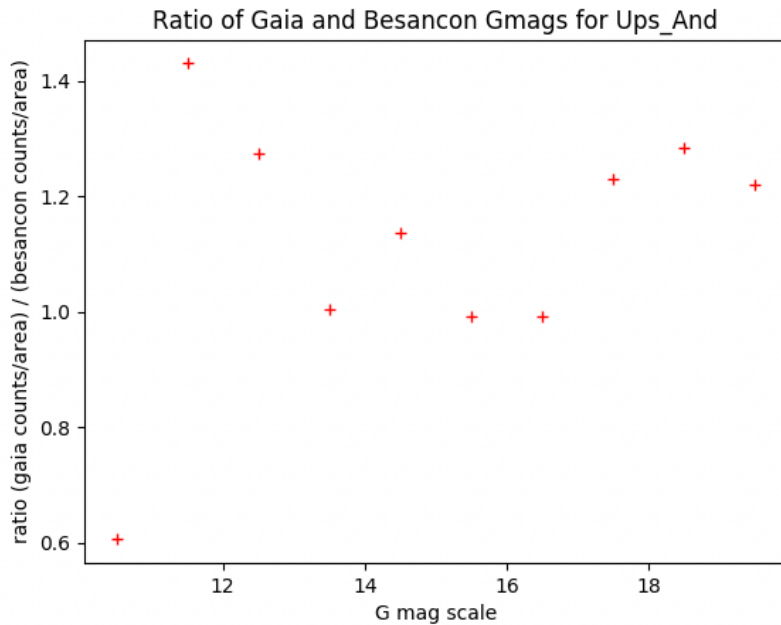


Figure 8 Ratio of Gaia counts per magnitude bin per square arcminute compared to Besançon model of the same at each magnitude bin for  $\nu$  And.

Table 4 Average ratio of Gaia to Besançon counts per square arcminute for magnitude bins of 15-20.

Target	Galactic Latitude (deg)	Ratio of Gaia to Besançon counts
14 Her	46.9449	1.018
47 Uma	63.3691	0.819
55 Cnc	37.6989	1.148
$\epsilon$ Eri	-48.0513	1.052
HD 142	-66.3866	1.022
HD 39091	-29.7763	0.990
HD 114613	24.889	0.995
HD 134987	27.3864	0.790
HD 154345	37.6635	0.979
HD 190360	-0.6725	0.518
HD 192310	-29.3975	0.815
HD 217107	-53.324	1.049
HD 219134	-3.1986	0.787
$\tau$ Ceti	-73.4397	0.746
$\nu$ And	-20.6662	1.144

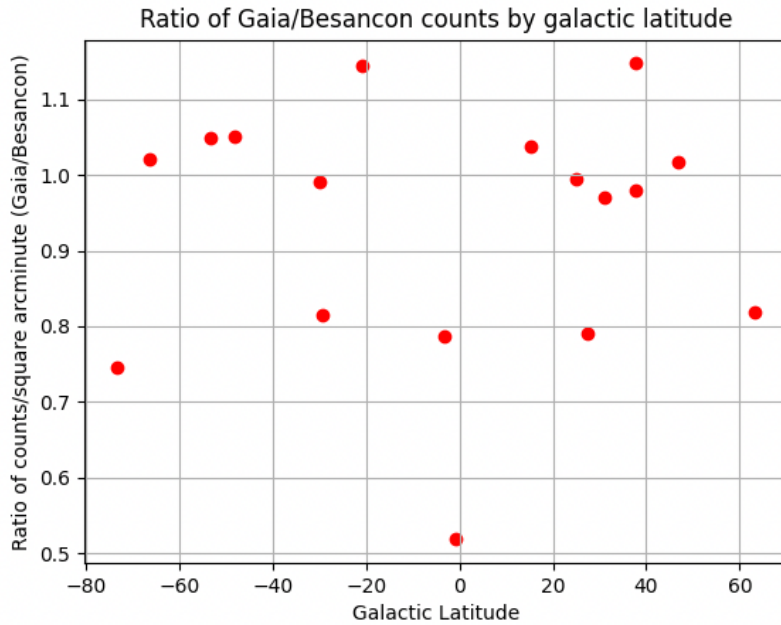


Figure 9 Ratio of Gaia to Besançon counts per square arcminute ( $15 < G < 20$ ) by galactic latitude. The ratio is within 5% of unity for about half of targets, and is no more than 25% off for any target. The exception is HD~190360, which is  $< 1$  degree from the galactic plane, where small-spatial-scale variability in both extinction and stellar counts may not be well-captured in the Besançon model.

Table 5 presents for each target, the number of stars found using Gaia in an 18 arcminute radius area around the target stars, the slope and intercept of the fitted lines as shown in Figure 5 and other figures for each target, and the expected number of objects at magnitudes of 20 and 24 per square arcminute. The magnitude bins cover integer ranges of magnitudes, so the magnitude 20 bin covers all magnitudes between 20 and 21, and the magnitude bin of 24 covers all magnitudes between 24 and 25. To get the expected number of sources within those bins, the following equation applies:

$$\log_{10}(\text{number of sources per square arcminute}) = \text{Slope} * \text{magnitude} + \text{Intercept}, \text{ keeping in mind this is a log relationship.}$$

Table 5 Gaia statistics for target stars. The slope and intercept values are those shown on the Gaia/Besançon plots with magnitudes vs. star counts per square arcminute. The last column is from the Besançon model, using the Besançon slope and intercept from the individual plots, just as a comparison to the predicted Gaia numbers at mag 24.

Target	Gaia sources	Gaia Slope	Gaia Intercept	Gaia Source density at mag 20	Gaia Source density at mag 24	Besançon source density at mag 24
14 Her	1460	0.180	-4.012	0.389	2.046	1.663
47 Uma	657	0.172	-4.202	0.175	0.855	0.796
55 Cnc	1242	0.145	-3.455	0.284	1.085	0.914
ε Eri	926	0.1797	-4.196	0.251	1.312	0.764
HD 142	1069	0.162	-3.848	0.250	1.117	1.270
HD 39091	3178	0.183	-3.701	0.919	4.972	4.256
HD 114613	5271	0.202	-3.817	1.695	10.925	9.795
HD 134987	5553	0.207	-3.871	1.811	12.129	21.878
HD 154345	1804	0.168	-3.667	0.486	2.277	2.366
HD 190360	49024	0.273	-4.272	15.334	189.304	277.971
HD 192310	5588	0.208	-3.911	1.738	11.754	19.815
HD 217107	1072	0.148	-3.506	0.282	1.101	1.422
HD 219134	20601	0.236	-3.871	6.964	61.045	88.920
τ Ceti	685	0.1996	-4.732	0.182	1.1419	0.820
υ And	3225	0.173	-3.480	0.955	4.696	2.710

Table 6 Using the values of stellar density per arcminute squared in the previous table, the number of sources which would be expected to fall in the Roman CGI full field of view are given for two different magnitudes.

Target	Predicted Gaia mag 20 stars in CGI FOV	Predicted Gaia mag 24 stars in CGI FOV	Predicted Besançon mag 20 stars in CGI FOV	Predicted Besançon mag 24 stars in CGI FOV
14 Her	4.40E-03	2.31E-02	4.00E-03	1.88E-02
47 Uma	1.98E-03	9.69E-03	2.18E-03	9.00E-03
55 Cnc	3.21E-03	1.22E-02	2.77E-03	1.03E-02
ε Eri	2.83E-03	1.48E-02	2.25E-03	8.64E-03
HD 142	2.84E-03	1.27E-02	2.94E-03	1.43E-02
HD 39091	1.04E-02	5.61E-02	9.96E-03	4.81E-02
HD 114613	1.91E-02	1.23E-01	1.84E-02	1.11E-01
HD 134987	2.05E-02	1.37E-01	2.97E-02	2.47E-01
HD 154345	5.50E-03	2.58E-02	5.59E-03	2.68E-02
HD 190360	1.74E-01	2.14E+00	3.03E-01	3.14E+00
HD 192310	1.96E-02	1.33E-01	2.74E-02	2.24E-01
HD 217107	3.19E-03	1.24E-02	3.46E-03	1.61E-02
HD 219134	7.88E-02	6.90E-01	1.04E-01	1.01E+00
τ Ceti	2.06E-03	1.29E-02	2.23E-03	9.28E-03
υ And	1.08E-02	5.31E-02	8.14E-03	3.07E-02

## 5. Conclusion

As will be seen in the analysis of the individual targets in Appendix A, Gaia shows few stars within the radius of the full CGI FOV ( $\sim 7.2$  arcseconds) of the target stars. In Table 6, the stellar densities in the full CGI field of view for magnitude 20 and 24 objects as expected from both Gaia and the Besançon models are shown. The Besançon value is a projection from the overlap region following the Gaia procedure, for comparison – since these projections invariably reside above the actual model at fainter magnitudes, the estimated density and hence contamination probability is conservative in overestimating the stellar density. These densities show that for most fields it is very unlikely that an object would randomly fall within the Roman CGI field of view.

The low Galactic latitude star HD 190360 shows that there are predicted to be around 2-3 stars of magnitude 24 in the full field of view, but if we consider only the smaller high contrast region, (radius 2.9 arcseconds) Gaia shows 0.348 stars of mag 24 and 0.028 stars of mag 20 in this region. This shows that there are not likely to be contaminating sources nearby enough to be a problem for the great majority of the expected observations, though at the lowest Galactic latitude, faint stellar background sources can be a concern.

The contamination analysis is based primarily on stellar statistics; however as seen in Figure 6, Figure 16, Figure 20, and Figure 43, (the stars with HSC data), a population of extragalactic sources is evident at the faintest relevant magnitudes. An effort was made to remove any spurious hits from the HSC catalogs, but there could still be a few such cases in the catalogs. Such spurious hits would contribute to, but not likely dominate the rise seen in the extragalactic sources. Modulo cosmic variance, the number of such sources is likely to be independent of galactic latitude and comparable to order of magnitude to the density of sources near these four stars. This density corresponds to an average of approximately 8 counts per square arcminute, which gives approximately one percent chance of finding an extragalactic background source within the Roman CGI high contrast region. These counts are loosely consistent with the galaxy counts found in previous work, e.g. Eliche-Moral 2006. This is on the verge of becoming significant, but is unlikely to be a major problem even at these bright magnitudes.

## Acknowledgements

Hubble Source Catalog: Based on observations made with the NASA/ESA Hubble Space Telescope, and obtained from the Hubble Legacy Archive, which is a collaboration between the Space Telescope Science Institute (STScI/NASA), the Space Telescope European Coordinating Facility (ST-ECF/ESAC/ESA) and the Canadian Astronomy Data Centre (CADC/NRC/CSA).

This work has made use of data from the European Space Agency (ESA) mission Gaia (<https://www.cosmos.esa.int/gaia>), processed by the Gaia Data Processing and Analysis Consortium (DPAC, <https://www.cosmos.esa.int/web/gaia/dpac/consortium>). Funding for the DPAC has been provided by national institutions, in particular the institutions participating in the Gaia Multilateral Agreement.

*This research has made use of the Besançon Galaxy Model,  
found here: [https://model.obs-besancon.fr/modele\\_home.php](https://model.obs-besancon.fr/modele_home.php)*

*This research has made use of the SIMBAD database,  
operated at CDS, Strasbourg, France.*

[2000,A&AS,143,9](#), "The SIMBAD astronomical database", Wenger et al.

Kasdin, N. et al. 2020, ‘The Nancy Grace Roman Space Telescope Coronagraph Instrument (CGI) technology demonstration’, Kasdin N. et al. *SPIE 11443*, SPIE Astronomical Telescopes and Instrumentation, 2020, Online Only, 15 December 2020.

Eliche-Moral, M. C., Balchells, M., Prieto, M., Garcia-Dabo, C. E., Erwin, P., Cristobal-Hornillos, D., 2006, ‘Goya Survey: U and B Number counts in the Groth Westphal Strip’. APJ 639:644-671

## APPENDIX

### A. Results for full target list

The appendix here shows results, plots and tables from an analysis of Gaia data and the Besançon model, and Hubble data where it is available, for the targets other than Upsilon Andromeda.

#### A.1. 14 Hercules

There is no Hubble data for 14 Hercules, so the analysis only includes the Gaia catalog and Besançon models. The first plot shows the comparison of the Gaia catalog to the Besançon models, showing source counts per square arcminute broken out by Gaia G magnitudes. The second figure and the table show the star positions from Gaia within one arcminute of the target star in 2026.

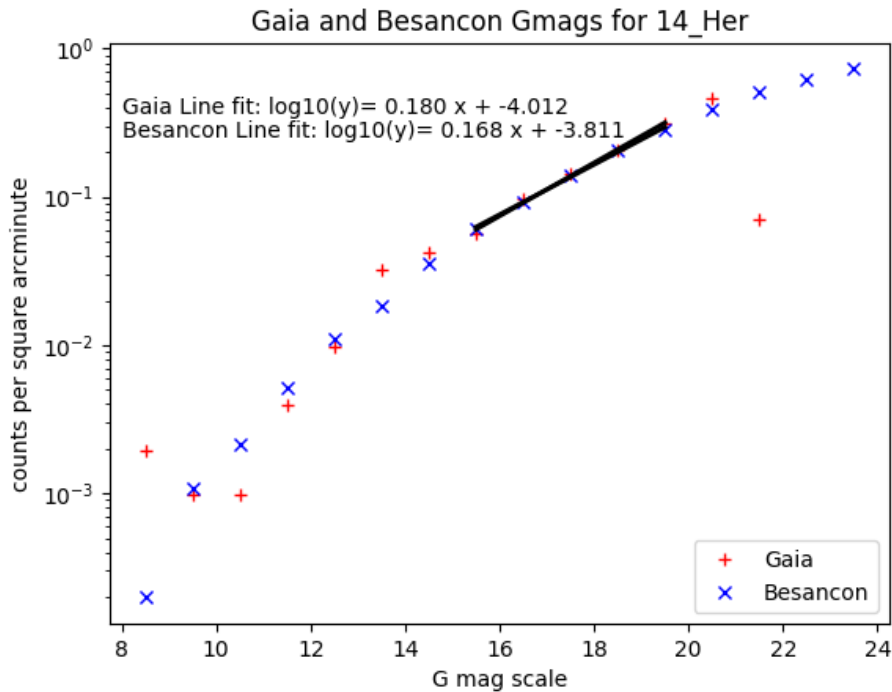


Figure 10 Gaia counts per magnitude bin per square arcminute compared to Besançon simulations of the same for 14 Her.

14 Her in 2026 is at RA, Dec of 16h10m24.631s +43d48m55.8183s as calculated from coordinates and proper motions found in SIMBAD in J2000 coordinates.

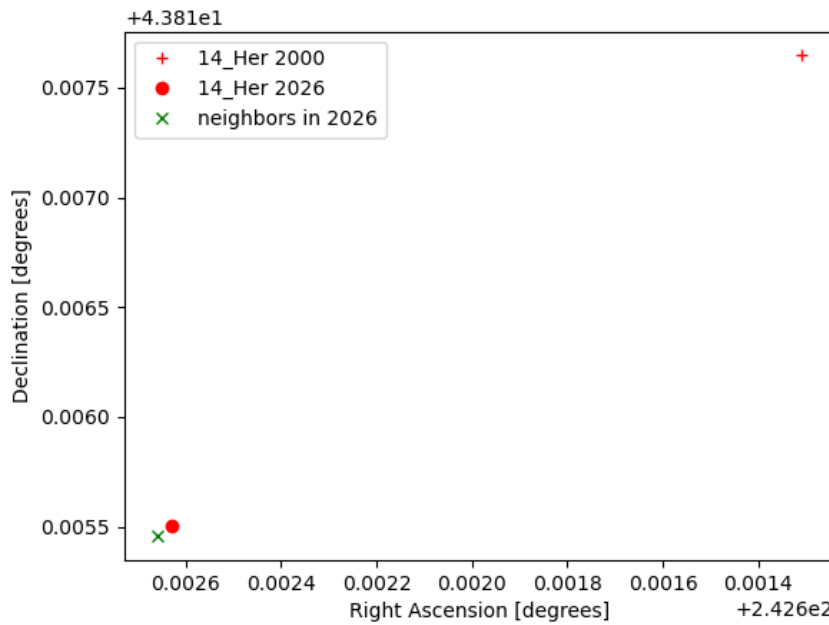


Figure 11 Positions of 14 Her in 2000 and 2026 compared with positions of other Gaia sources within one arcminute.

Table 7 Positions of stars within one arcminute of 14 Her in 2026. Only the star itself is within 1 arcmin.

Source ID	Distance (arcsec)	RA	Dec	G mag
<b>1385293808145621504</b>	<b>0.19393</b>	<b>16h10m24.6385s</b>	<b>+43d48m55.6424s</b>	<b>6.3793</b>

## A.2 47 Ursae Majoris

There is no Hubble data for 47 Ursae Majoris, so the analysis only includes the Gaia catalog and Besançon models. The first plot shows the comparison of the Gaia catalog to the Besançon models, showing source counts per square arcminute broken out by Gaia G magnitudes. The second figure and the table show the star positions from Gaia within one arcminute of the target star in 2026.

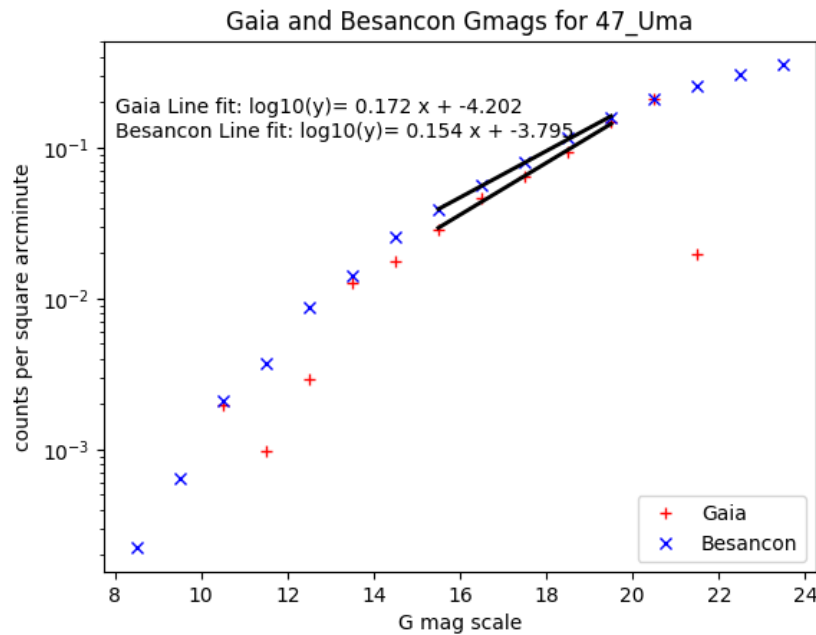


Figure 12 Gaia counts per magnitude bin per square arcminute compared to Besançon simulations of the same for 47 UMa.

The position of 47 UMa in 2026 in RA, Dec is 10h59m27.2495s +40d25m50.3504s as calculated from coordinates and proper motions found in SIMBAD in J2000 coordinates.

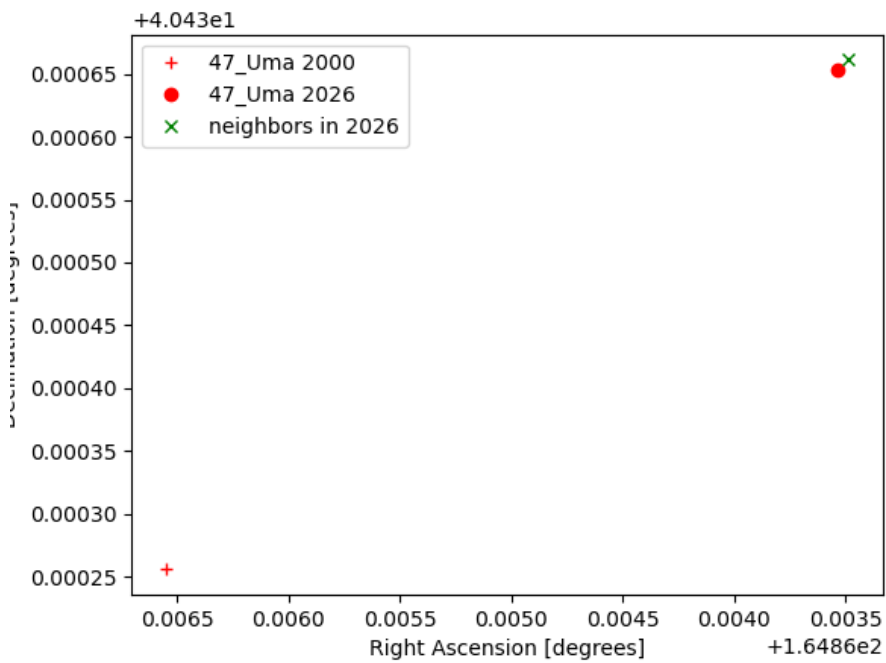


Figure 13 Positions of 47 UMa in 2000 and 2026 compared with positions of other Gaia sources within one arcminute.

Table 8 Positions of stars within one arcminute of 47 UMa in 2026. Only the star itself is within 1 arcmin.

Source ID	Distance (arcseconds)	RA	Dec	G mag
777254360337133312	0.14988	10h59m27.2366s	+40d25m50.3803s	4.8306

### A.3 55 Cancri

There is Hubble data for 55 Cancri, images both on the star and in parallel fields. The proper motion of the star can be shown in a single WFC3 IR image centered on the star. This image shown below on the left is from 2015, ico517siq\_drz.fits. The green circle shows the position of the star in 2000, while the red circle shows where the star will be in 2026.

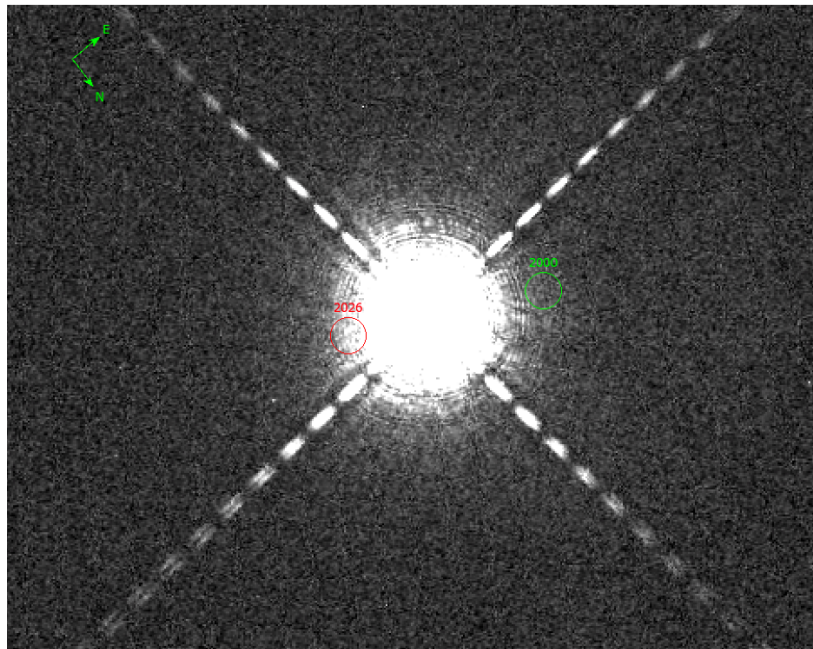


Figure 14 Hubble WFC3 IR image of 55 Cancri taken in 2015. The circle in green shows the 2000 position, while the circle in red shows where the star will be in 2026.

There are several parallel fields taken within 18 arcminutes of the target star. There are three WFPC2 F606W fields, and one ACS F775W image. Two of those WFPC2 images and the ACS fields combine only two images to have exposure times of 2000 seconds or less, while one WFPC2 image consists of 30 individual combined images with a total exposure time of 31553 seconds. Looking at this combined image in the Hubble Source catalog shows 128 sources total, which gives a total of approximately 22 sources per square arcminute in the combined image, since a WFPC2 image has a 5.692 square arcminute field of view. If we divide this out using the concentration index (CI) value to separate possible stars from probable galaxies with CI values  $< 1.2$  being more likely to be stars and CI values  $> 1.2$  more likely to be galaxies (as was done in the analysis above, the breakdown is 9 sources with a CI less than 1.2 and 119 with a CI greater than 19).

Table 9 Comparison of total sources in WFPC2 combined image (total and broken out by CI value) compared to the Gaia catalog for the area around 55 Cancri.

Catalog being used	Area of coverage (square arcsec)	Total number of sources	Source density per square arcminute
Total of WFPC2	5.7	128	22.5
Sources with CI < 1.2	5.7	9	1.6
Sources with CI > 1.2	5.7	119	20.9
Gaia (within r=18 arcmin)	1017.9	1242	1.2
Besançon	25920.0	124109	4.8

This table shows that the Hubble catalog contains many more sources than the Gaia catalog, but also that most of the sources found in this particular field of view are more likely to be galaxies than stars. If only stars are compared, then Gaia and the Hubble Source catalog are in closer agreement.

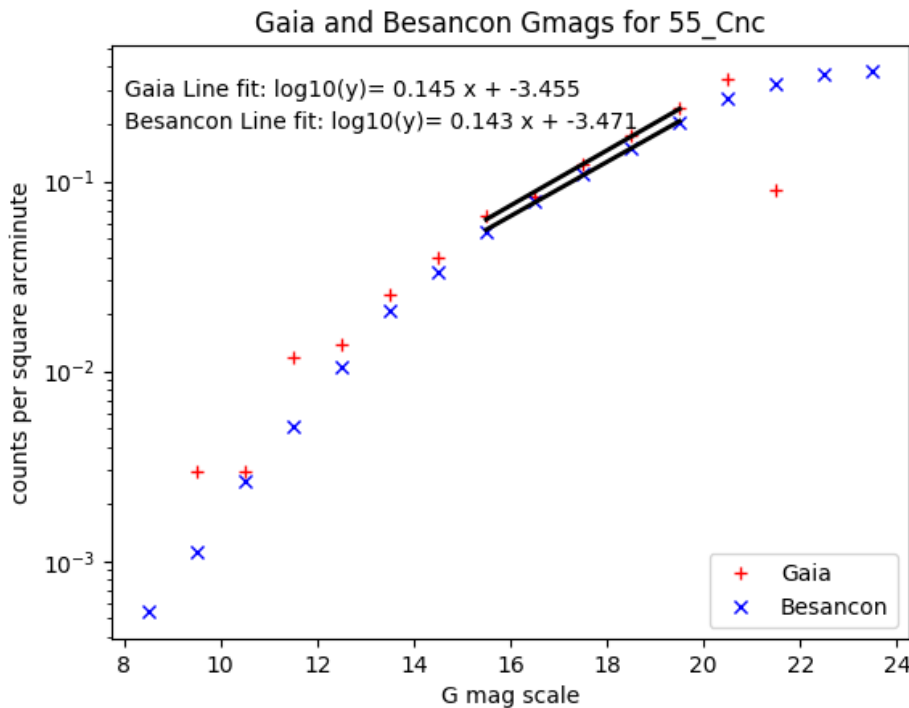


Figure 15 Gaia counts per magnitude bin per square arcminute compared to Besançon simulations of the same for 55 Cnc.

Adding in the WFPC2 data described above to Figure 14 gives us Figure 15, which shows that the Hubble WFPC2 magnitudes for the stars (CI< 1.2) are well aligned with Gaia and the Besançon catalogs, while the galaxies dominate at the faintest magnitudes. To convert from WFPC2 F606W magnitudes to Gaia G magnitudes, an offset of 0.8 was subtracted.

$$\text{Gmag} = \text{WFPC2mag} - 0.8$$

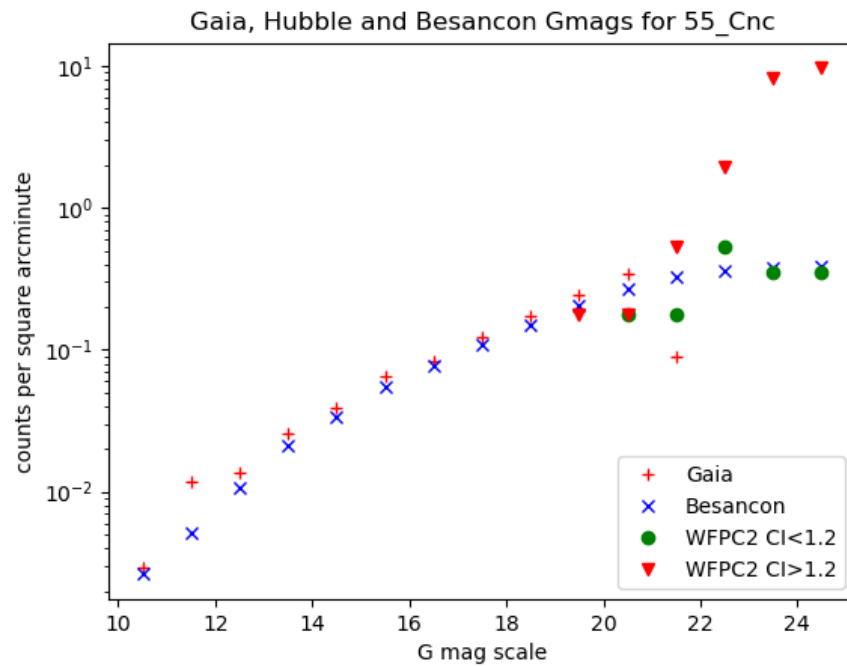


Figure 16 Comparison of Gaia, WFPC2 and Besançon source counts per magnitudes per square arcminute near 55 Cancri. The WFPC2 data is separated out into point sources ( $CI < 1.2$ ) and extended sources ( $CI \geq 1.2$ )

The position of 55 Cnc in 2026 in RA, Dec is 08h52m34.8542s +28d19m44.876s as calculated from coordinates and proper motions found in SIMBAD in J2000 coordinates.

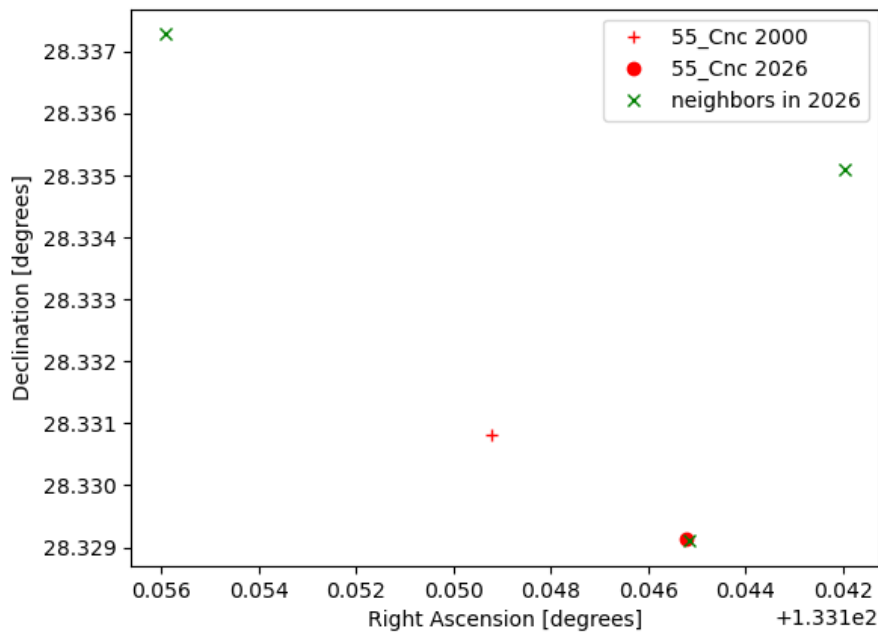


Figure 17 Positions of 55 Cnc in 2000 and 2026 compared with positions of other Gaia sources within one arcminute.

Table 10 Positions of stars within one arcminute of 55 Cnc in 2026. Target star in bold italics.

Source ID	Distance	RA	Dec	G mag
<b>704967037090946688</b>	<b>0.26233</b>	<b>08h52m34.8362s</b>	<b>+28d19m44.7652s</b>	<b>5.7144</b>
704967037089999232	23.8737	08h52m34.0675s	+28d20m06.3719s	20.6613
704967140168773888	44.8516	08h52m37.4243s	+28d20m14.204s	19.2226

#### A.4 Epsilon Eridani

Epsilon Eridani also has data taken with Hubble, which allows us to use both the Hubble Source Catalog and the Hubble Legacy archive to examine images of the source itself and the parallel fields around it to see how well the statistics from Hubble match those of Gaia and the Besançon simulated catalog.

The image below is a 1996 WFPC2/PC combined image from the HLA, hst\_0683\_02\_wfpc2\_total\_wf\_sci.fits, centered on the target. The green circle indicates the positions of the star in 2000 and the red circle indicates the position in 2026.

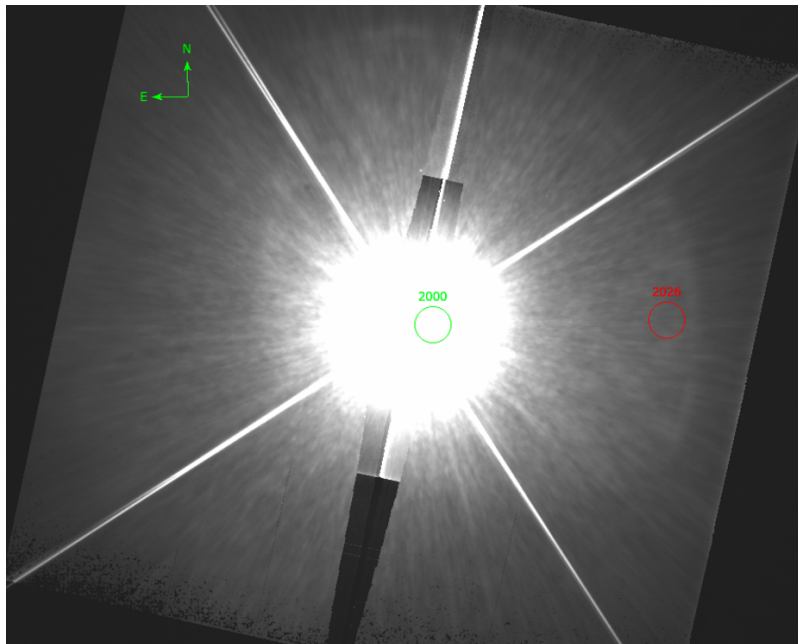


Figure 18 Hubble WFPC2/PC HLA image of  $\epsilon$  Eri taken in 1996. The circle in green shows the 2000 position, while the circle in red shows where the star will be in 2026.

A wider shot with the central region washed out by the bright star shows the surrounding area with one or two fainter stars and several background galaxies.

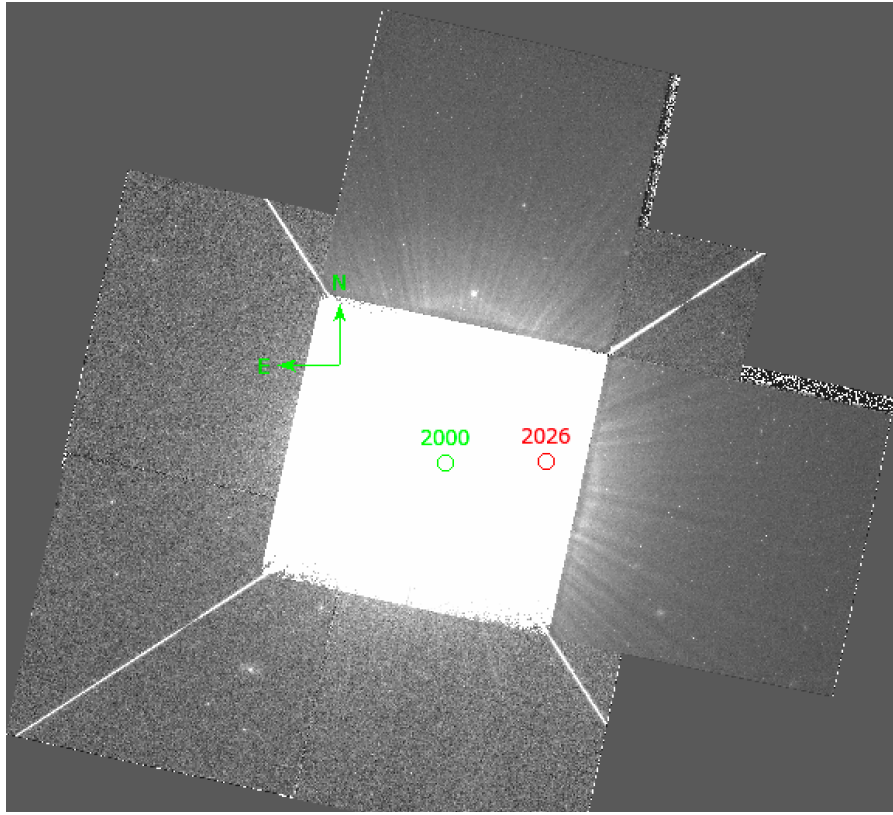


Figure 19 Hubble WFPC2/PC HLA image of  $\epsilon$  Eri taken in 1996. The circle in green shows the 2000 position, while the circle in red shows where the star will be in 2026. The wider field of view shows the background galaxies and one or two fainter stars.

In the Hubble Legacy archive, there are two ACS F775W images within the 18 arcminute radius. Using the Hubble source catalog, we can obtain a catalog of sources.

By limiting the sources to only those found in more than one ACS image, there were 905 stars found in the two ACS images. While there are some known spurious sources (multiple sources counted in the arms of a large spiral galaxy for instance), this catalog can be compared to what was found with Gaia and predicted with the Besançon simulation. There are a large number of galaxies in this image, which is shown when the sources are broken out by concentration index. CI values less than 1.2 are assumed to be point sources, while CI values greater than 1.2 are assumed to be more elongated and likely galaxies.

Table 11 Comparison of total sources in two fields of ACS combined images (total and broken out by CI value) compared to the Gaia catalog for the area around  $\varepsilon$  Eri.

Catalog being used	Area of coverage (square arcsec)	Total number of sources	Source density per square arcminute
Total of ACS	22.7	905	40
Sources with $CI < 1.2$	22.7	92	4.1
Sources with $CI > 1.2$	22.7	813	35.9
Gaia	1017.9	926	0.9
Besançon	33120	137986	4.2

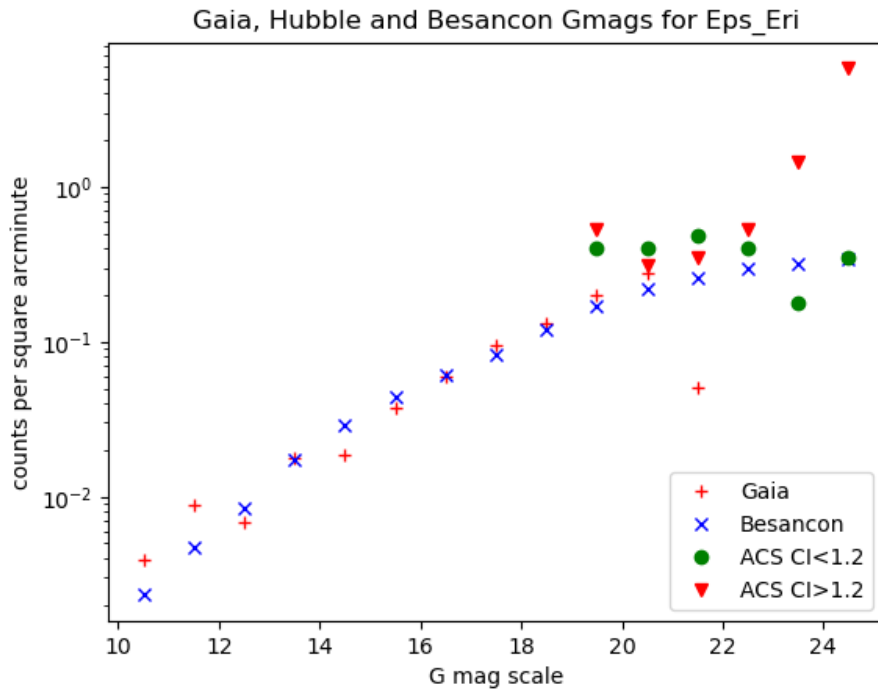


Figure 20 Comparison of Gaia, ACS and Besançon source counts per magnitudes per square arcminute near  $\varepsilon$  Eri. The ACS data is separated out into point sources ( $CI < 1.2$ ) and extended sources ( $CI \geq 1.2$ ).

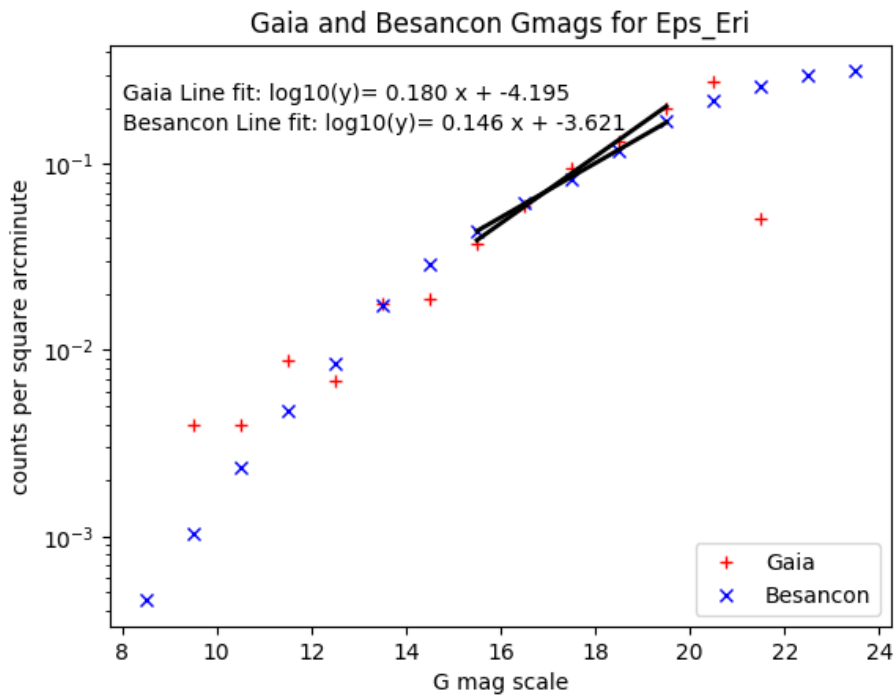


Figure 21 Gaia counts per magnitude bin per square arcminute compared to Besançon simulations of the same for ε Eri.

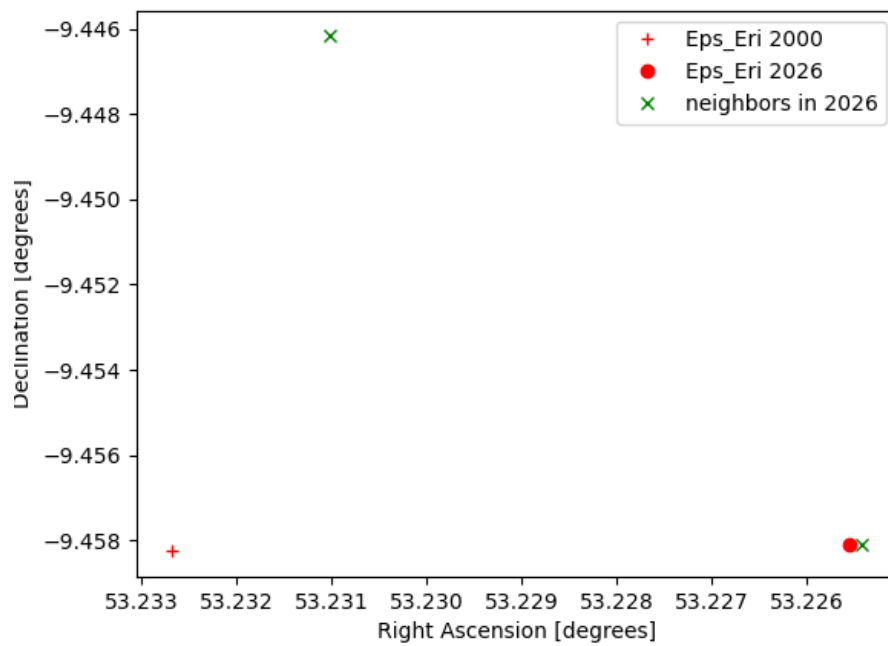


Figure 22 Positions of  $\epsilon$  Eri in 2000 and 2026 compared with positions of other Gaia sources within one arcminute.

Table 12 Positions of stars within one arcminute of  $\varepsilon$  Eri in 2026. Target star in bold italics.

Source ID	Dist	RA	Dec	G mag
<b>5164707970261630080</b>	<b>0.49153</b>	<b>03h32m54.0982s</b>	<b>-09d27m29.1945s</b>	<b>3.3691</b>
5164708142060320768	47.18	03h32m55.4431s	-09d26m46.2211s	17.628

### A.5 HD 142

There is no Hubble data for HD 142, so the analysis only includes the Gaia catalog and Besançon models. The first plot shows the comparison of the Gaia catalog to the Besançon models, showing source counts per square arcminute broken out by Gaia G magnitudes. The second figure and the table show the star positions from Gaia within one arcminute of the target star in 2026.

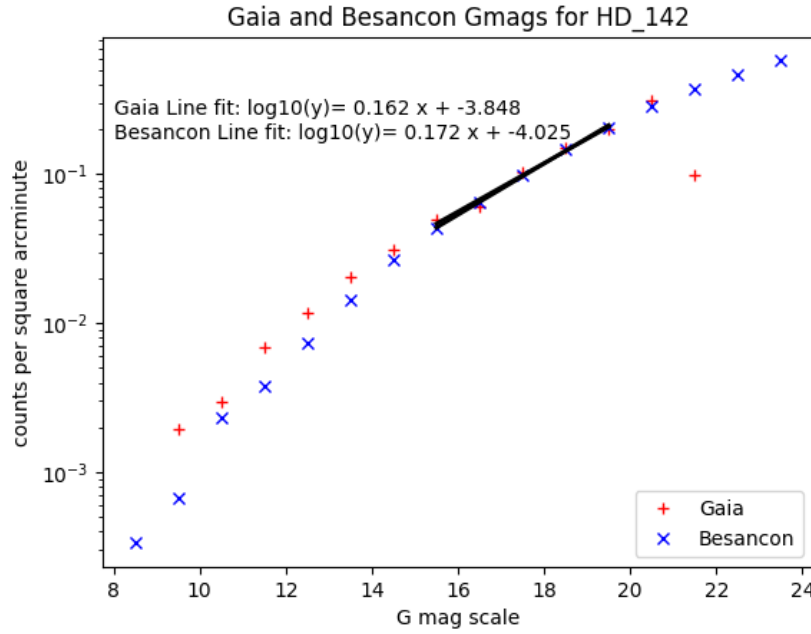


Figure 23 Gaia counts per magnitude bin per square arcminute compared to Besançon simulations of the same for HD 142.

The position of HD 142 in 2026 in RA, Dec is 00h06m20.6977s -49d04m31.7s as calculated from coordinates and proper motions found in SIMBAD in J2000 coordinates.

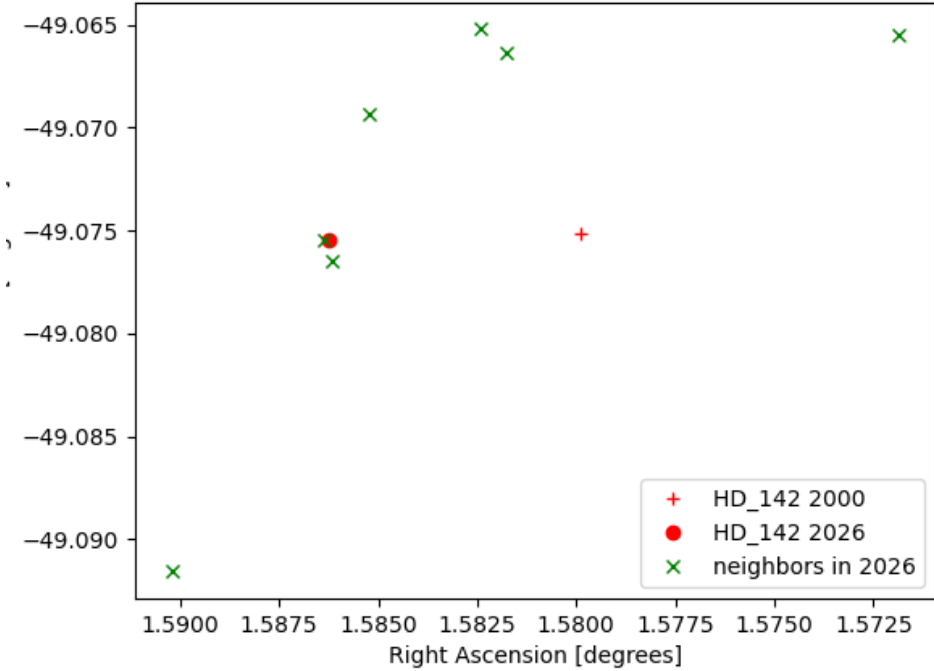


Figure 24 Positions of HD 142 in 2000 and 2026 compared with positions of other Gaia sources within one arcminute.

Table 13 Positions of stars within one arcminute of HD 142 in 2026. Target star in bold italics.

Source ID	Distance (arcseconds)	RA	Dec	G mag
4976894891564743168	58.744	00h06m21.6513s	-49d05m29.6921s	13.4579
<b>4976894960284258048</b>	<b>0.2854</b>	<b>00h06m20.7262s</b>	<b>-49d04m31.7525s</b>	<b>5.5647</b>
4976894960284258176	3.67068	00h06m20.677s	-49d04m35.365s	10.5334
4976895166441959808	34.4445	00h06m19.6275s	-49d03m58.9003s	19.8742
4976895166442687744	22.0543	00h06m20.4566s	-49d04m09.7733s	18.9162
4976895162145914368	37.9892	00h06m19.7818s	-49d03m54.7925s	12.304
4976895235160081792	49.4881	00h06m17.2428s	-49d03m55.6944s	20.5782

## A.6 HD 39091

There is no Hubble data for HD 39091, so the analysis only includes the Gaia catalog and Besançon models. The first plot shows the comparison of the Gaia catalog to the Besançon models, showing source counts per square arcminute broken out by Gaia G magnitudes. The second figure and the table show the star positions from Gaia within one arcminute of the target star in 2026.

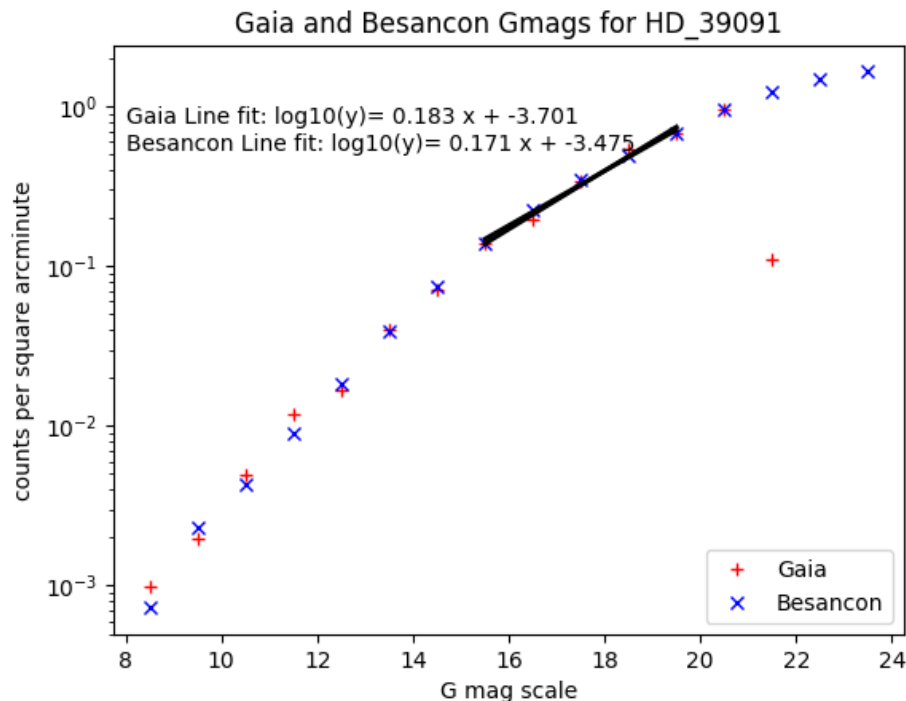


Figure 25 Gaia counts per magnitude bin per square arcminute compared to Besançon simulations of the same for HD 39091.

The position of HD 39091 in 2026 in RA, Dec is 05h37m13.1469s -80d27m41.566s as calculated from coordinates and proper motions found in SIMBAD in J2000 coordinates.

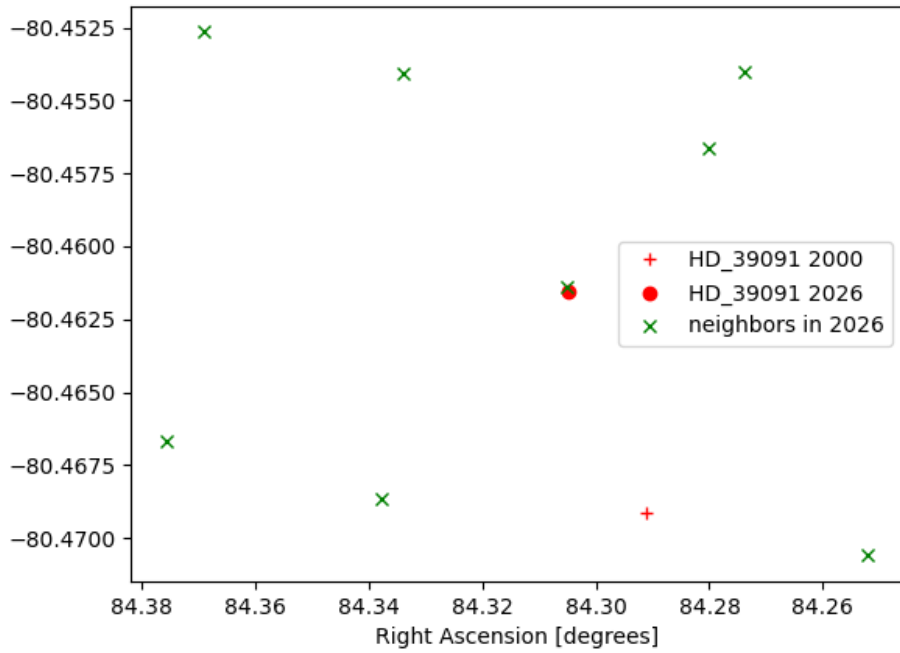


Figure 26 Positions of HD 39091 in 2000 and 2026 compared with positions of other Gaia sources within one arcminute.

Table 14 Positions of stars within one arcminute of HD 39091 in 2026. Target star in bold italics.

Source ID	Distance (arcseconds)	RA	Dec	G mag
4623036934091503232	22.9469	05h37m07.2486s	-80d27m23.9164s	18.3499
4623036899732204032	45.3085	05h37m00.4829s	-80d28m14.1685s	20.6984
4623036865373916160	32.2556	05h37m21.0681s	-80d28m07.1206s	19.6821
4623036934091936640	32.7732	05h37m05.6841s	-80d27m14.5526s	20.7209
<b>4623036865373793408</b>	<b>0.54777</b>	<b>05h37m13.2043s</b>	<b>-80d27m41.0371s</b>	<b>5.4907</b>
4623036865372029312	46.1935	05h37m30.1729s	-80d28m00.1066s	20.049
4623036968453008640	31.949	05h37m20.1274s	-80d27m14.7436s	17.6043
4623036964157027072	49.9753	05h37m28.5763s	-80d27m09.5457s	18.3

### A.7 HD 114613

There is no Hubble data for HD 114613, so the analysis only includes the Gaia catalog and Besançon models. The first plot shows the comparison of the Gaia catalog to the Besançon models, showing source counts per square arcminute broken out by Gaia G magnitudes. The second figure and the table show the star positions from Gaia within one arcminute of the target star in 2026.

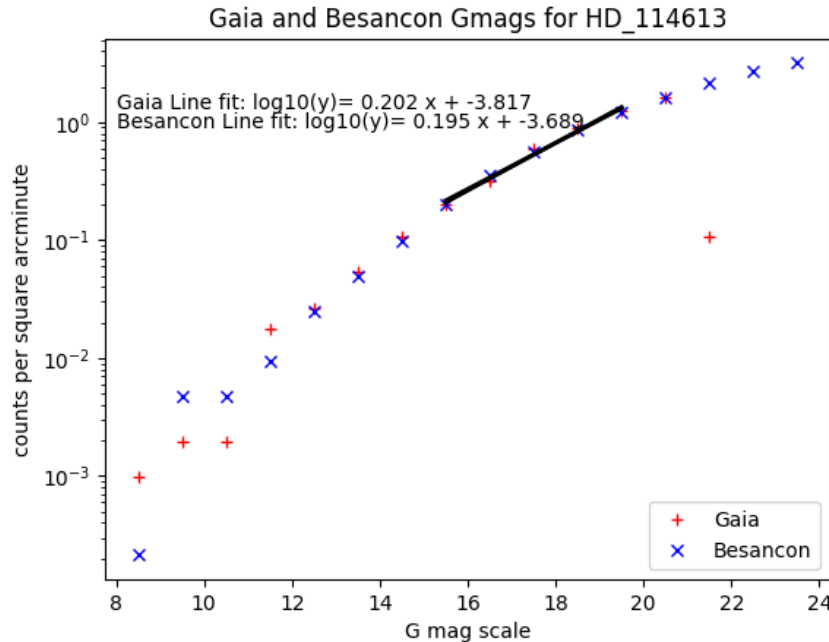


Figure 27 Gaia counts per magnitude bin per square arcminute compared to Besançon simulations of the same for HD 114613.

The position of HD 114613 in 2026 in RA, Dec is 13h12m02.3478s -37d48m09.6915s as calculated from coordinates and proper motions found in SIMBAD in J2000 coordinates.

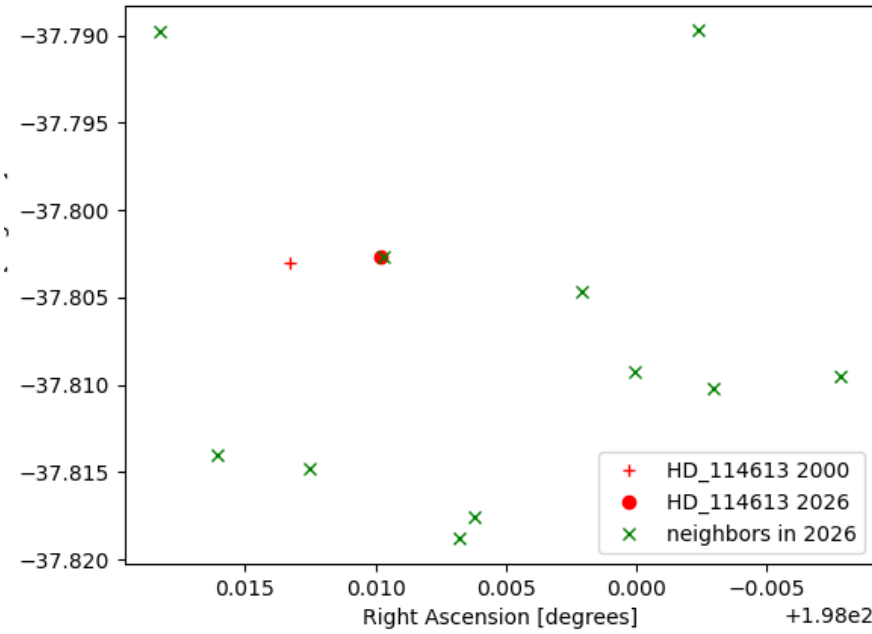


Figure 28 Positions of HD 114613 in 2000 and 2026 compared with positions of other Gaia sources within one arcminute.

Table 15 Positions of stars within one arcminute of HD 114613 in 2026. Target star in bold italics.

Source ID	Distance (arcseconds)	RA	Dec	G mag
6141740737212770176	58.6572	13h12m01.6255s	-37d49m07.7208s	18.1022
6141740737211402880	54.4518	13h12m01.4888s	-37d49m03.1832s	20.1172
6141740805930881408	45.18	13h11m59.2918s	-37d48m36.7003s	20.1659
6141740801637679616	55.9515	13h11m58.1115s	-37d48m34.3893s	18.0182
6141740805932250624	36.3211	13h12m00.0175s	-37d48m33.2825s	16.9388
6141742214681522176	44.5623	13h12m03.8516s	-37d48m50.5352s	16.6065
<b><i>6141742283401003264</i></b>	<b><i>0.21366</i></b>	<b><i>13h12m02.33s</i></b>	<b><i>-37d48m09.6579s</i></b>	<b><i>4.6041</i></b>
6141742317759093120	52.5585	13h12m04.3927s	-37d47m23.0554s	19.7557
6141742214679865344	44.2042	13h12m03.0005s	-37d48m53.2137s	16.741
6141742283399941120	23.1168	13h12m00.4953s	-37d48m16.9261s	18.08
6141742489557784448	58.1325	13h11m59.4242s	-37d47m23.0169s	19.8122

### A.8 HD 134987

There is no Hubble data for HD 134987, so the analysis only includes the Gaia catalog and Besançon models. The first plot shows the comparison of the Gaia catalog to the Besançon models, showing source counts per square arcminute broken out by Gaia G magnitudes. The second figure and the table show the star positions from Gaia within one arcminute of the target star in 2026.

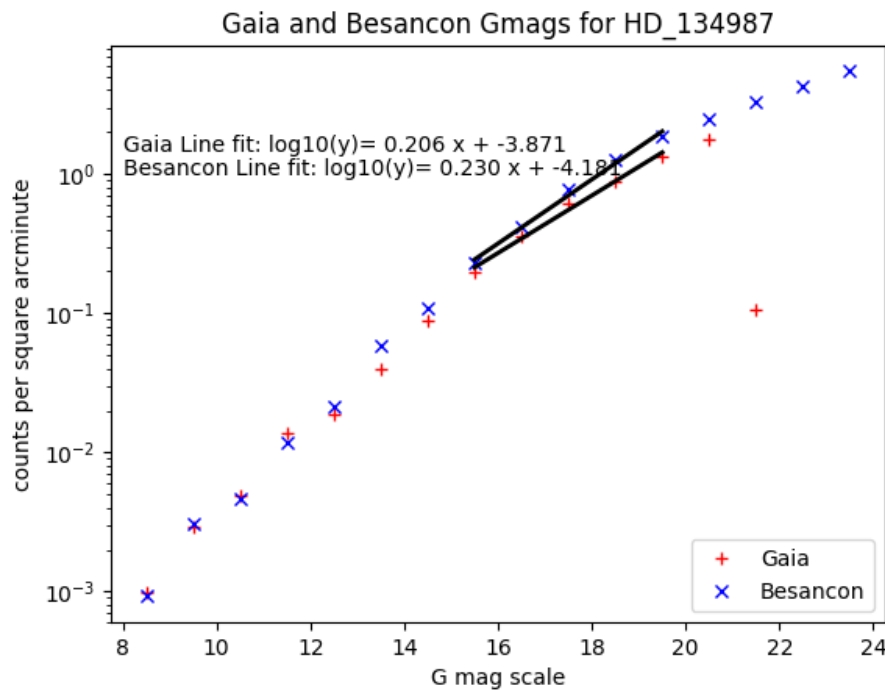


Figure 29 Gaia counts per magnitude bin per square arcminute compared to Besançon simulations of the same for HD 134987.

The position of HD 134987 in 2026 in RA, Dec is 15h13m27.8995s -25d18m35.6008s as calculated from coordinates and proper motions found in SIMBAD in J2000 coordinates.

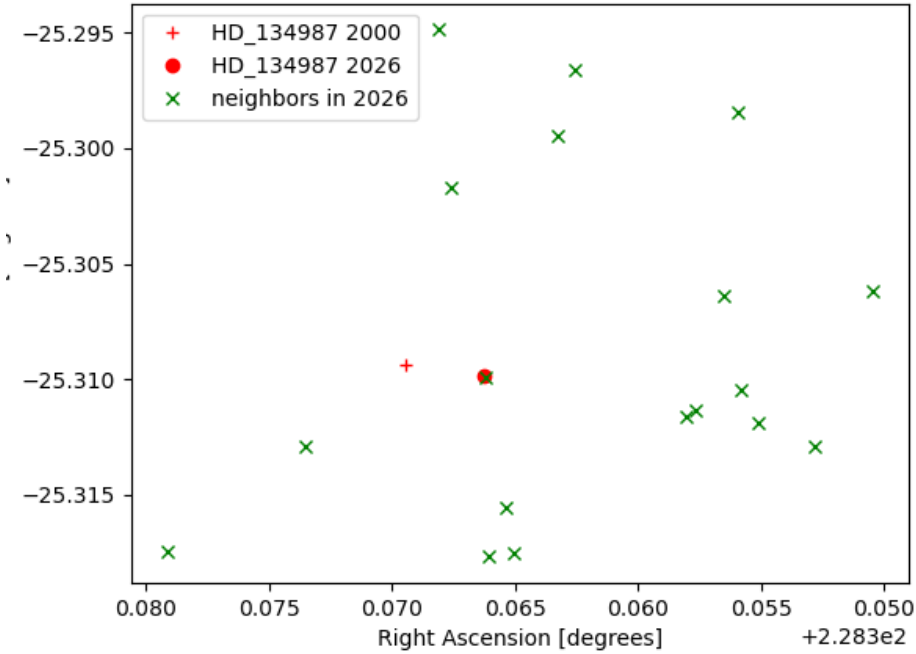


Figure 30 Positions of HD 134987 in 2000 and 2026 compared with positions of other Gaia sources within one arcminute.

Table 16 Positions of stars within one arcminute of HD 134987 in 2026. Target star in bold italics.

Source ID	Distance (arcseconds)	RA	Dec	G mag
6226694571852593792	27.727	15h13m27.6182s	-25d19m03.0643s	20.623
6226694571852594304	28.1001	15h13m27.8595s	-25d19m03.6957s	20.6672
6226694571852171648	36.8607	15h13m25.2339s	-25d18m42.8257s	20.2321
6226694571852171264	28.4234	15h13m25.8386s	-25d18m40.7861s	18.9553
<b>6226694571859532800</b>	<b>0.20438</b>	<b>15h13m27.8848s</b>	<b>-25d18m35.6464s</b>	<b>6.2855</b>
6226694567557774976	20.6197	15h13m27.6893s	-25d18m56.0225s	17.8468
6226694571852171904	33.9348	15h13m25.4022s	-25d18m37.789s	19.1932
6226694571852171392	27.3736	15h13m25.9331s	-25d18m41.7891s	19.7601
6226694571852171520	44.9868	15h13m24.6823s	-25d18m46.5853s	19.7234
6226694773715602688	53.1791	15h13m24.1043s	-25d18m22.2082s	18.6414
6226694778010603776	33.9635	15h13m25.5704s	-25d18m23.1117s	18.9884
6226694773715604352	53.1817	15h13m25.4247s	-25d17m54.3455s	19.4535
6226695980608801664	50.0686	15h13m30.9983s	-25d19m02.8284s	18.8917
6226696045026524928	29.8436	15h13m28.2188s	-25d18m06.073s	19.4181
6226695980601424640	26.0881	15h13m29.6512s	-25d18m46.3885s	20.6085
6226696255486715648	49.3556	15h13m27.023s	-25d17m47.6979s	17.8724

6226696255486827520	38.7852	15h13m27.1902s	-25d17m58.0274s	17.2242
6226696255479356288	54.4068	15h13m28.3505s	-25d17m41.5389s	19.3674

### A.9 HD 154345

There is no Hubble data for HD 154345, so the analysis only includes the Gaia catalog and Besançon models. The first plot shows the comparison of the Gaia catalog to the Besançon models, showing source counts per square arcminute broken out by Gaia G magnitudes. The second figure and the table show the star positions from Gaia within one arcminute of the target star in 2026.

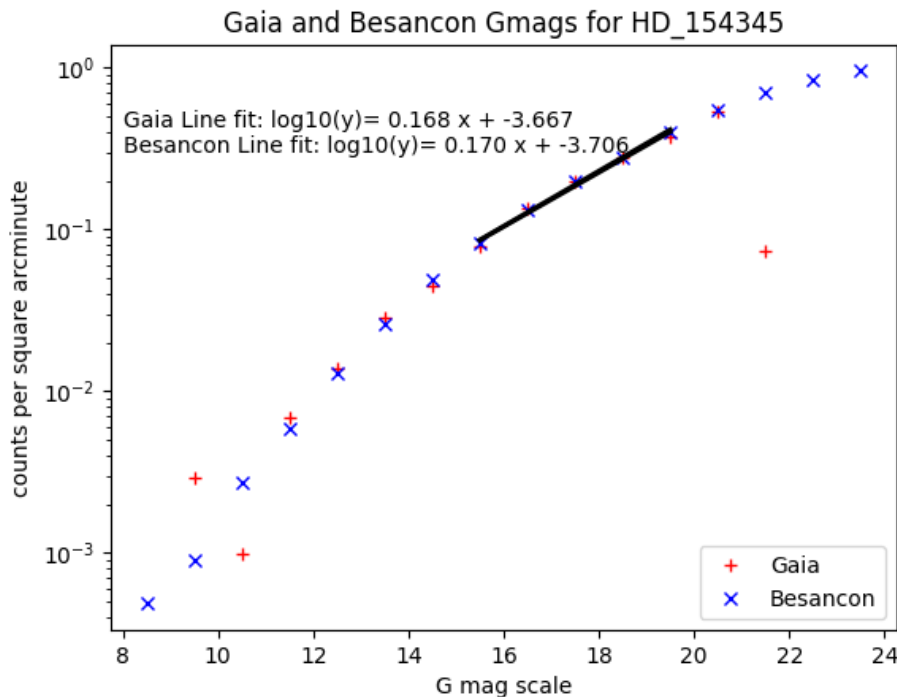


Figure 31 Gaia counts per magnitude bin per square arcminute compared to Besançon simulations of the same for HD 154345.

The position of HD 154345 in 2026 in RA, Dec is 17h02m36.7172s +47d05m16.9614s as calculated from coordinates and proper motions found in SIMBAD in J2000 coordinates.

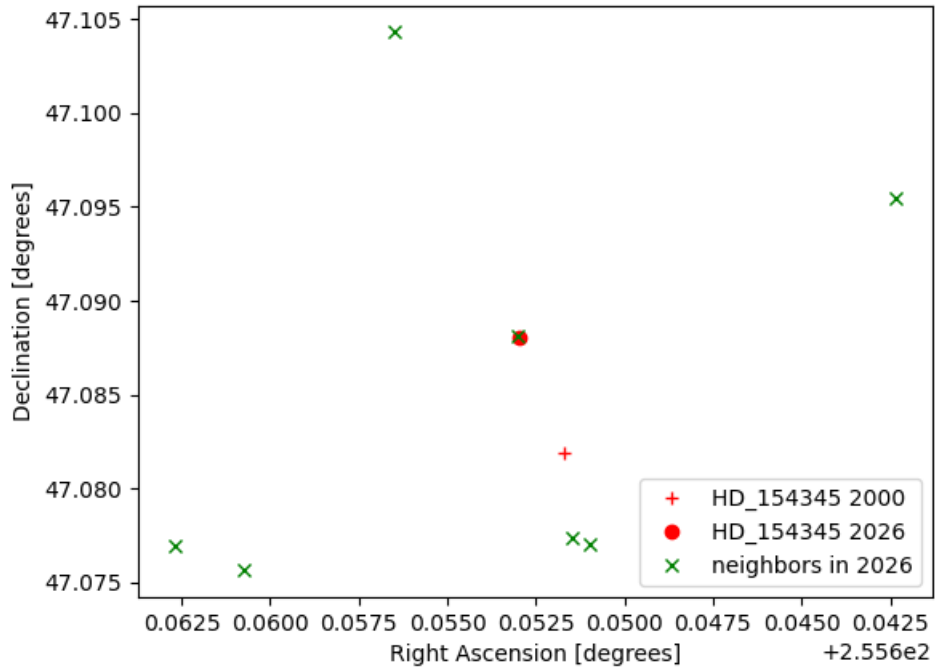


Figure 32 Positions of HD 154345 in 2000 and 2026 compared with positions of other Gaia sources within one arcminute.

Table 17 Positions of stars within one arcminute of HD 154345 in 2026. Target star in bold italic.

Source ID	Distance (arcseconds)	RA	Dec	G mag
1359938348454023936	46.4644	17h02m39.0496s	+47d04m37.069s	20.357
1359938348454024064	48.4967	17h02m38.574s	+47d04m32.3269s	18.995
1359938520252717056	39.8187	17h02m36.2322s	+47d04m37.452s	18.0025
<b><i>1359938520253565952</i></b>	<b><i>0.43034</i></b>	<b><i>17h02m36.7236s</i></b>	<b><i>+47d05m17.3868s</i></b>	<b><i>6.5677</i></b>
1359938520253565184	38.5834	17h02m36.3569s	+47d04m38.554s	16.5179
1359939344886446464	37.4041	17h02m34.1579s	+47d05m43.7176s	19.7019
1359939374952210048	59.132	17h02m37.5626s	+47d06m15.4599s	20.8453

## A.10 HD 160691

There were no Besançon simulations run for this target, so the comparison plot for Gaia and Besançon do not exist. There is no Hubble data for HD 160691, so the analysis only includes the Gaia catalog. The figure and the table show the star positions from Gaia within one arcminute of the target star in 2026.

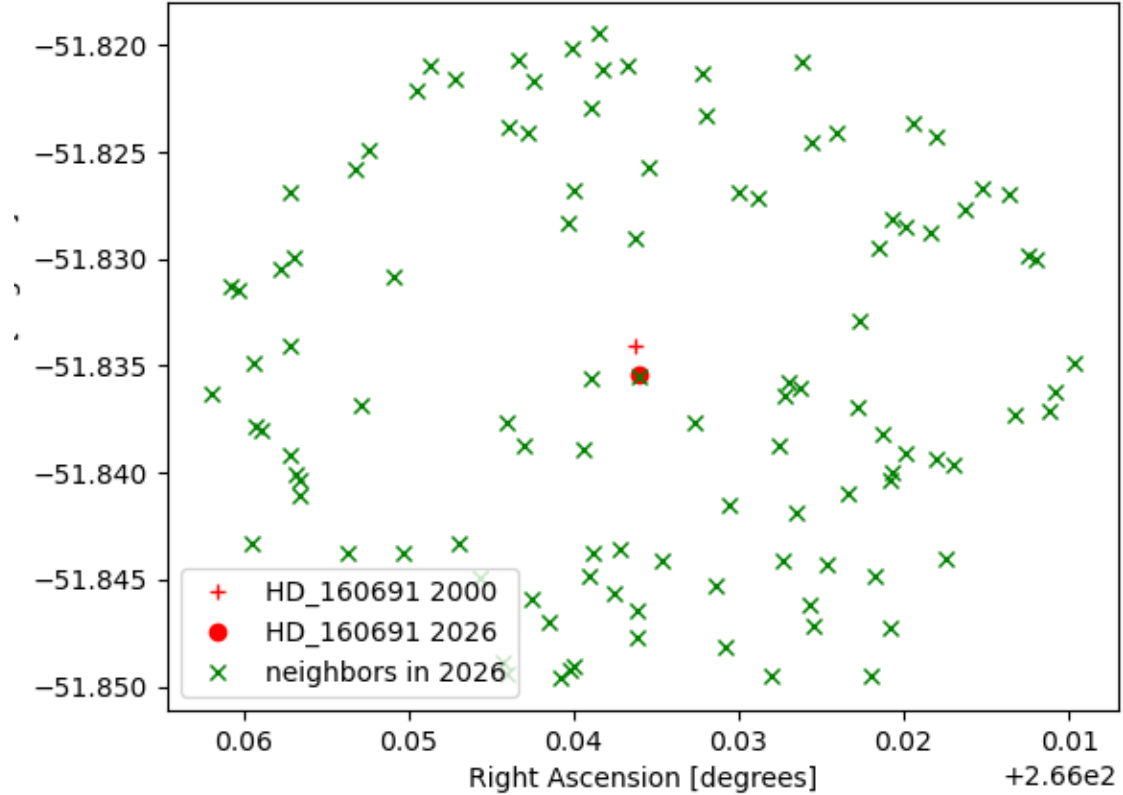


Figure 33 Positions of HD 160691 in 2000 and 2026 compared with positions of other Gaia sources within one arcminute.

Table 18 Positions of stars within one arcminute of HD 160691 in 2026. Target star in bold italics.

Source ID	Distance (arcseconds)	RA	Dec	G mag
<b>5945941905576552064</b>	<b>0.09581</b>	<b>17h44m08.6599s</b>	<b>-51d50m07.6504s</b>	<b>4.9046</b>
5945941905576873472	6.31182	17h44m09.3401s	-51d50m07.9785s	14.9915
5945941905569456512	10.9238	17h44m07.8435s	-51d50m15.4264s	16.4316
5946035742006792064	23.0674	17h44m08.6924s	-51d49m44.4894s	17.9404
5945941905562631680	14.4635	17h44m09.4609s	-51d50m19.9717s	14.8977
5945941905569222656	19.2842	17h44m10.5566s	-51d50m15.4975s	18.1123
5945941905569228288	19.9302	17h44m06.5403s	-51d50m10.8681s	16.6731

5945941905576800256	20.2583	17h44m06.4793s	-51d50m08.8135s	14.9379
5945941905569222144	19.2942	17h44m10.3128s	-51d50m19.2934s	17.67
5946035737715783296	27.3942	17h44m09.6878s	-51d49m41.8683s	16.6439
5945941905562677632	21.9244	17h44m06.3071s	-51d50m09.7477s	18.7326
5945941901271338880	22.4174	17h44m06.6164s	-51d50m19.5355s	14.5173
5946035742023713280	32.4071	17h44m09.5849s	-51d49m36.3008s	18.7669
5946035742023275392	33.6631	17h44m07.1914s	-51d49m36.7703s	17.859
5945941871209484544	24.9812	17h44m07.3331s	-51d50m29.2959s	18.4466
5946035742023275648	33.9983	17h44m06.9216s	-51d49m37.6213s	15.596
5946035742024159872	35.0265	17h44m08.5029s	-51d49m32.559s	19.6234
5945941905569231104	31.1399	17h44m05.4505s	-51d49m58.3723s	18.8706
5945941901271338368	30.0793	17h44m05.4687s	-51d50m12.9815s	17.0474
5945941905562619520	29.4287	17h44m08.9152s	-51d50m36.8889s	17.7787
5946023990992752512	36.8566	17h44m12.205s	-51d49m50.8503s	15.9747
5945941901271339136	30.6157	17h44m09.3048s	-51d50m37.5829s	17.3596
5945941871217025024	31.5034	17h44m06.3734s	-51d50m30.8589s	17.249
5945941871209483136	31.3753	17h44m08.3015s	-51d50m38.7531s	17.6581
5945941871209750016	34.4697	17h44m05.1016s	-51d50m17.5544s	19.2797
5945941974296277120	38.9538	17h44m05.1537s	-51d49m46.0919s	16.8212
5945941871209486848	34.592	17h44m05.6224s	-51d50m27.6455s	18.3791
5946023990974817792	37.7416	17h44m12.6976s	-51d50m12.4941s	18.7399
5946035742005343104	43.4967	17h44m10.2581s	-51d49m26.6565s	18.324
5945941871209716864	34.6352	17h44m09.372s	-51d50m41.5568s	19.8187
5946035742005344896	44.5732	17h44m07.6806s	-51d49m23.9174s	18.3769
5946035742005342976	45.1591	17h44m10.5413s	-51d49m25.8963s	19.7713
5946035742008662784	45.5533	17h44m09.3333s	-51d49m22.4304s	20.6462
5945941974282190592	43.0427	17h44m04.973s	-51d49m41.3978s	18.8708
5945941935631076480	38.0497	17h44m04.9545s	-51d50m23.9198s	17.479
5945941939936502656	38.4836	17h44m04.765s	-51d50m20.8683s	19.0567
5945941901271339776	37.2799	17h44m11.2755s	-51d50m35.8835s	19.0664
5945941939936292608	38.3411	17h44m04.9847s	-51d50m25.1403s	18.799
5945941871216811776	36.7634	17h44m06.5667s	-51d50m38.7786s	17.9894
5945941974282191872	43.77	17h44m04.7759s	-51d49m42.6739s	19.1204
5945941871209483264	36.8252	17h44m07.5382s	-51d50m42.8802s	18.7271
5945941871216806016	36.9105	17h44m09.0042s	-51d50m44.3278s	17.3887
5946035742008300672	45.6879	17h44m06.1411s	-51d49m28.2881s	20.5369
5945941974289607936	46.0624	17h44m04.4246s	-51d49m43.4744s	20.6961
5945941905576541824	40.2302	17h44m10.9728s	-51d50m41.6032s	14.6803

5945941871209481984	39.5316	17h44m08.6718s	-51d50m47.0863s	19.1092
5945941939922425856	42.5437	17h44m04.328s	-51d50m21.6046s	19.4973
5945941905562598016	40.3638	17h44m10.2012s	-51d50m45.3095s	19.6427
5945941866911600128	40.7952	17h44m05.9176s	-51d50m39.4596s	18.4401
5946035742005346048	48.8398	17h44m05.778s	-51d49m26.674s	19.1097
5946023990992752000	47.017	17h44m13.7064s	-51d50m02.7282s	19.0851
5946035742005859072	51.4612	17h44m07.7195s	-51d49m16.8387s	20.1476
5946035742005343616	51.553	17h44m10.1871s	-51d49m17.982s	19.2856
5945930154546276736	43.5193	17h44m12.0781s	-51d50m37.4004s	20.0763
5946035742006801792	51.7665	17h44m09.182s	-51d49m16.0145s	20.2998
5946035742005344768	52.0439	17h44m08.8018s	-51d49m15.5274s	19.7463
5945941939936693376	44.9614	17h44m04.0875s	-51d50m22.5544s	20.6963
5945941866911601024	43.2268	17h44m09.9542s	-51d50m49.0861s	17.2813
5946024025337882368	51.4907	17h44m12.7787s	-51d49m32.9997s	20.689
5946023986685261952	50.5628	17h44m13.6774s	-51d49m47.7019s	18.0676
5946024025335058816	52.481	17h44m12.5839s	-51d49m29.7178s	19.9848
5945941871216805120	44.1589	17h44m08.6881s	-51d50m51.7131s	13.5659
5946023990974818688	51.3546	17h44m13.8514s	-51d49m49.602s	18.8057
5945941866911600256	45.1779	17h44m06.173s	-51d50m46.4072s	18.0819
5945941974287131904	52.0278	17h44m03.9141s	-51d49m39.7883s	19.767
5946023990978150656	48.8646	17h44m13.7326s	-51d50m20.8948s	20.5968
5946023990974742784	48.9814	17h44m13.6248s	-51d50m24.3567s	19.9014
5945941871217138944	46.5976	17h44m05.2164s	-51d50m41.5019s	20.9736
5945930154529261056	49.008	17h44m13.5869s	-51d50m25.3631s	20.263
5946035776366538112	55.5456	17h44m10.3941s	-51d49m14.3844s	20.3668
5946035742005344384	55.8005	17h44m09.6096s	-51d49m12.4521s	19.0764
5946035776365587328	55.7045	17h44m11.3138s	-51d49m17.574s	20.3248
5946023990974816896	51.8054	17h44m14.2462s	-51d50m05.6831s	18.6523
5945930154542359424	49.8665	17h44m13.5716s	-51d50m27.9268s	21.0499
5945930154538696704	49.2614	17h44m12.8851s	-51d50m37.4518s	19.8596
5945941871217101184	47.3292	17h44m07.3946s	-51d50m53.4066s	20.7406
5946035776365081088	56.5514	17h44m11.8899s	-51d49m19.5764s	18.8032
5946023990974816384	51.637	17h44m14.1402s	-51d50m16.8861s	19.9265
5945941939928968832	51.2533	17h44m03.1797s	-51d50m14.3463s	20.1949
5946035742008301312	57.7196	17h44m09.2277s	-51d49m10.0751s	20.8396
5946035737715782016	57.1461	17h44m06.2751s	-51d49m14.8616s	16.8913
5945941974288935296	56.2711	17h44m04.6524s	-51d49m25.2964s	20.2383
5945941866907658112	48.5223	17h44m06.0986s	-51d50m49.8707s	18.3937

5946023990974816512	52.3147	17h44m14.2279s	-51d50m16.1721s	19.199
5946024025334557824	56.0899	17h44m13.7285s	-51d49m36.9076s	19.6317
5945941974292362880	55.8955	17h44m03.6664s	-51d49m36.2343s	20.7011
5945941974288712320	56.7775	17h44m04.335s	-51d49m27.3584s	19.9265
5946023990992752256	55.7465	17h44m14.4721s	-51d49m53.2023s	17.9279
5945941871202852608	49.7668	17h44m09.5977s	-51d50m56.5582s	20.3354
5946035776365081216	59.2196	17h44m11.6829s	-51d49m15.3819s	19.0692
5945941974282209664	56.3559	17h44m02.9857s	-51d49m47.3344s	20.8716
5945941939936537344	51.7512	17h44m04.197s	-51d50m38.6481s	20.2121
5945941871202852736	50.4714	17h44m09.6456s	-51d50m57.1941s	18.5215
5946023990974817920	56.976	17h44m14.5935s	-51d49m52.6548s	19.921
5945941974282209792	57.0175	17h44m02.8823s	-51d49m48.0076s	19.4362
5945941871209716352	51.7623	17h44m10.6152s	-51d50m56.0447s	20.3619
5945941974296041472	58.5687	17h44m03.2598s	-51d49m37.1611s	19.6096
5945941871216802048	52.1627	17h44m09.787s	-51d50m58.6626s	15.6888
5945941935627136640	55.6993	17h44m02.6872s	-51d50m13.6352s	16.1987
5945941939930770816	56.1463	17h44m02.6106s	-51d50m10.3407s	20.711
5946023990974816256	57.6954	17h44m14.8755s	-51d50m10.8079s	19.5768
5945941871202841344	53.3949	17h44m10.5629s	-51d50m57.9558s	19.8124
5945941871202884992	53.6364	17h44m06.7185s	-51d50m58.0811s	19.5996
5945941871202913280	54.3182	17h44m05.0029s	-51d50m49.997s	19.8621
5945941939928970880	58.9187	17h44m02.3077s	-51d50m05.5736s	20.1843
5945930154532040064	59.228	17h44m14.2764s	-51d50m35.8228s	18.76
5945941768130267776	59.7688	17h44m05.261s	-51d50m58.3455s	20.0679

### A.11 HD 190360

There is no Hubble data for HD 190360, so the analysis only includes the Gaia catalog and Besançon models. The first plot shows the comparison of the Gaia catalog to the Besançon models, showing source counts per square arcminute broken out by Gaia G magnitudes. The second figure and the table show the star positions from Gaia within one arcminute of the target star in 2026.

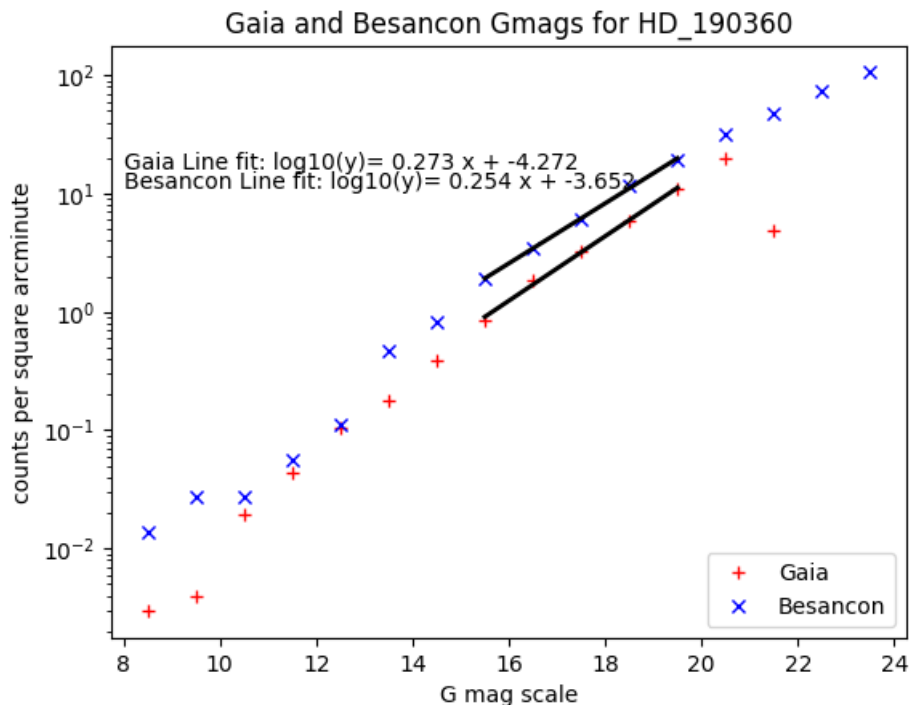


Figure 34 Gaia counts per magnitude bin per square arcminute compared to Besançon simulations of the same for HD 190360.

The position of HD 190360 in 2026 in RA, Dec is 20h03m38.7721s +29d53m34.8264s as calculated from coordinates and proper motions found in SIMBAD in J2000 coordinates.

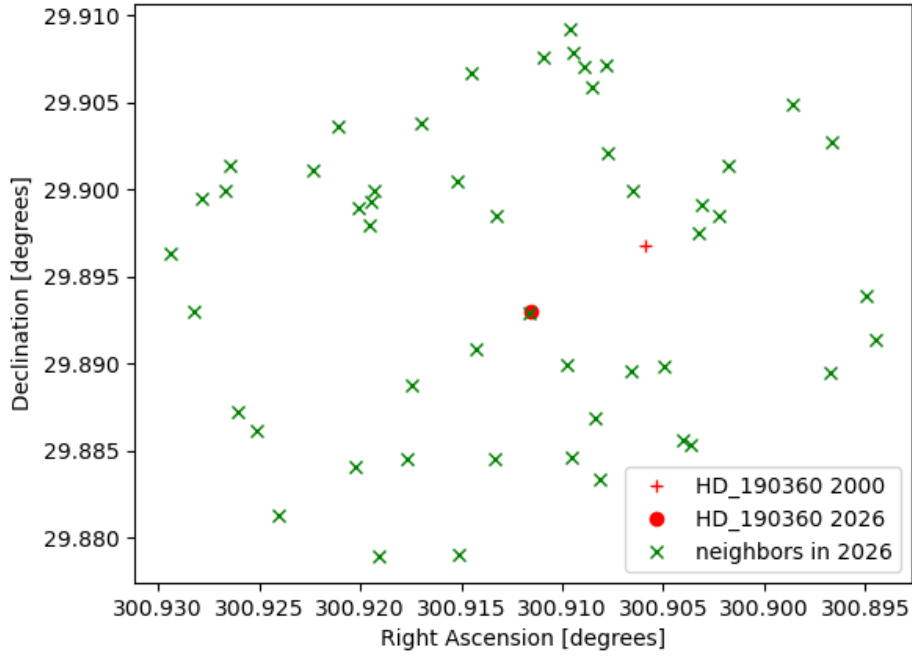


Figure 35 Positions of HD 190360 in 2000 and 2026 compared with positions of other Gaia sources within one arcminute.

Table 19 Positions of stars within one arcminute of HD 190360 in 2026. Target star in bold italic.

Source ID	Distance (arcseconds)	RA	Dec	G mag
2029432765329761664	31.1654	20h03m39.2026s	+29d53m04.1681s	20.764
2029432765330391040	11.6278	20h03m39.4284s	+29d53m26.9295s	19.1538
2029432765327143552	36.0466	20h03m40.2361s	+29d53m04.2183s	20.4234
2029432765328343040	30.8263	20h03m38.2952s	+29d53m04.6303s	20.4926
2029432761021700096	55.996	20h03m40.577s	+29d52m43.988s	19.6152
2029432761021271040	51.5863	20h03m39.6298s	+29d52m44.4607s	18.7672
2029432761025276032	23.9488	20h03m40.1884s	+29d53m19.5201s	19.2462
2029432761025277056	42.1644	20h03m40.8568s	+29d53m02.5344s	20.5324
2029432761025278464	57.3239	20h03m41.7632s	+29d52m52.7214s	20.6072
2029432765329890560	36.2575	20h03m37.9518s	+29d53m00.1738s	21.1459
2029432868406359680	53.5394	20h03m42.4109s	+29d53m59.8757s	19.9149
2029432864100921856	55.359	20h03m42.3394s	+29d54m05.0376s	19.7199
2029432868407576320	56.0215	20h03m42.6835s	+29d53m58.3072s	20.3794
2029432864104494080	49.0618	20h03m42.0374s	+29d53m10.2548s	20.1551
2029432864100489728	49.7828	20h03m42.2535s	+29d53m14.1252s	16.5718
2029432864100493056	52.157	20h03m42.7828s	+29d53m34.919s	17.7616

2029432868405734912	57.0936	20h03m43.0627s	+29d53m46.9298s	18.0439
2029433521244006784	30.569	20h03m36.7724s	+29d53m50.8958s	20.8184
2029433516939518208	19.938	20h03m37.5757s	+29d53m22.358s	19.8272
2029433589962082176	42.7916	20h03m36.4274s	+29d54m04.8513s	20.4503
2029433521244691968	34.2551	20h03m36.7506s	+29d53m56.7889s	19.571
2029433585659030144	58.2236	20h03m35.2039s	+29d54m09.9973s	20.3816
2029433585659030656	58.7987	20h03m35.6611s	+29d54m17.4966s	19.5716
2029433486889134976	53.7004	20h03m34.6669s	+29d53m29.0166s	19.8075
2029433521244261376	23.6316	20h03m37.1866s	+29d53m23.2797s	20.1811
2029433521248542464	24.2345	20h03m38.0099s	+29d53m12.7116s	17.013
<b>2029433521248546304</b>	<b>0.42062</b>	<b>20h03m38.7974s</b>	<b>+29d53m34.565s</b>	<b>5.5336</b>
2029433521248551424	29.4112	20h03m37.5673s	+29d53m59.7178s	13.7435
2029433521240806656	35.511	20h03m36.9734s	+29d53m08.1078s	21.0218
2029433585658992128	52.0102	20h03m34.78s	+29d53m37.9795s	20.4412
2029433516939515776	47.8681	20h03m35.2204s	+29d53m22.2559s	18.8095
2029433516939517440	37.0356	20h03m36.8757s	+29d53m07.197s	18.5789
2029433516939518720	12.3187	20h03m38.3471s	+29d53m23.8173s	14.0642
2029433521243180928	35.1966	20h03m36.5331s	+29d53m54.6008s	19.7191
2029433624320003712	33.5665	20h03m40.6793s	+29d53m57.4452s	19.1763
2029433693040092544	52.1705	20h03m37.8727s	+29d54m25.6692s	20.1795
2029433624322377344	29.1519	20h03m39.6449s	+29d54m01.6778s	20.5879
2029433693040092032	54.0621	20h03m38.2603s	+29d54m28.4774s	18.9553
2029433624321823232	50.205	20h03m39.479s	+29d54m24.1826s	19.1294
2029433620018771200	47.4362	20h03m38.0486s	+29d54m21.3202s	20.2029
2029433688738248576	58.5633	20h03m38.3154s	+29d54m33.0878s	18.4581
2029433620018771968	52.5572	20h03m38.6247s	+29d54m27.3486s	18.3042
2029433620018774656	48.5126	20h03m41.0657s	+29d54m13.0877s	20.9952
2029433624327755776	34.7516	20h03m40.6247s	+29d53m59.8719s	17.459
2029433624322965888	30.6891	20h03m40.6984s	+29d53m52.5558s	20.5654
2029433624322373888	42.5533	20h03m40.0801s	+29d54m13.8324s	20.6814
2029433624327767552	34.8674	20h03m37.8615s	+29d54m07.6214s	17.9071
2029433624327769344	51.1189	20h03m38.1403s	+29d54m25.281s	18.3089
2029433620018734464	20.618	20h03m39.1876s	+29d53m54.724s	20.3351
2029433620018736000	34.2073	20h03m40.8175s	+29d53m56.3362s	18.7808
2029433624327915264	44.6335	20h03m41.3593s	+29d54m04.1561s	19.0579

### A.12 HD 192310

There is no Hubble data for HD 192310, so the analysis only includes the Gaia catalog and Besançon models. The first plot shows the comparison of the Gaia catalog to the Besançon models, showing source counts per square arcminute broken out by Gaia G magnitudes. The second figure and the table show the star positions from Gaia within one arcminute of the target star in 2026.

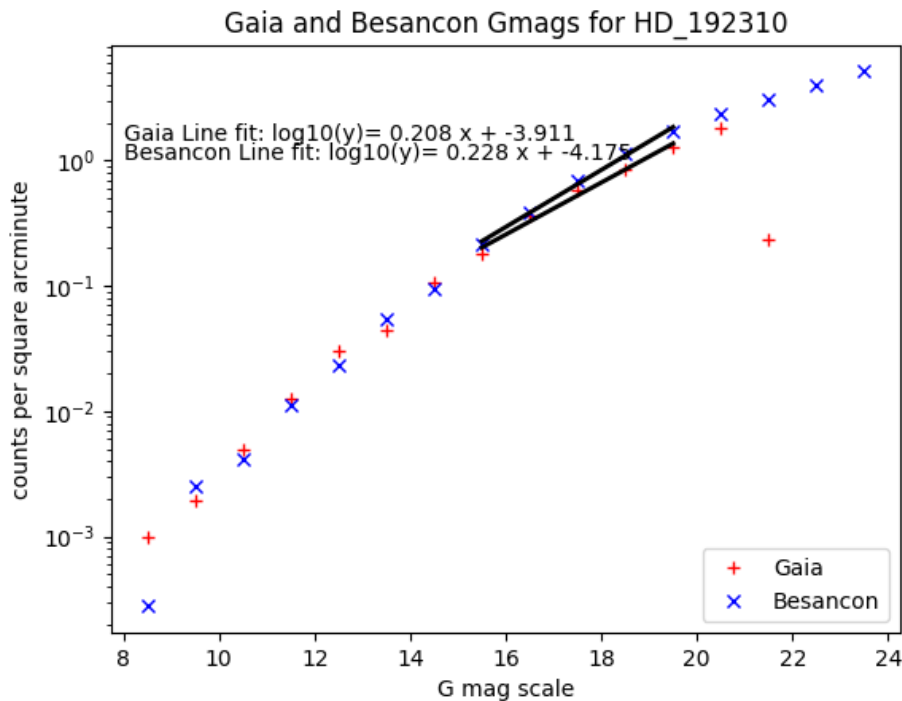


Figure 36 Gaia counts per magnitude bin per square arcminute compared to Besançon simulations of the same for HD 192310.

The position of HD 192310 in 2026 in RA, Dec is 20h15m19.8091s -27d02m03.418s as calculated from coordinates and proper motions found in SIMBAD in J2000 coordinates.

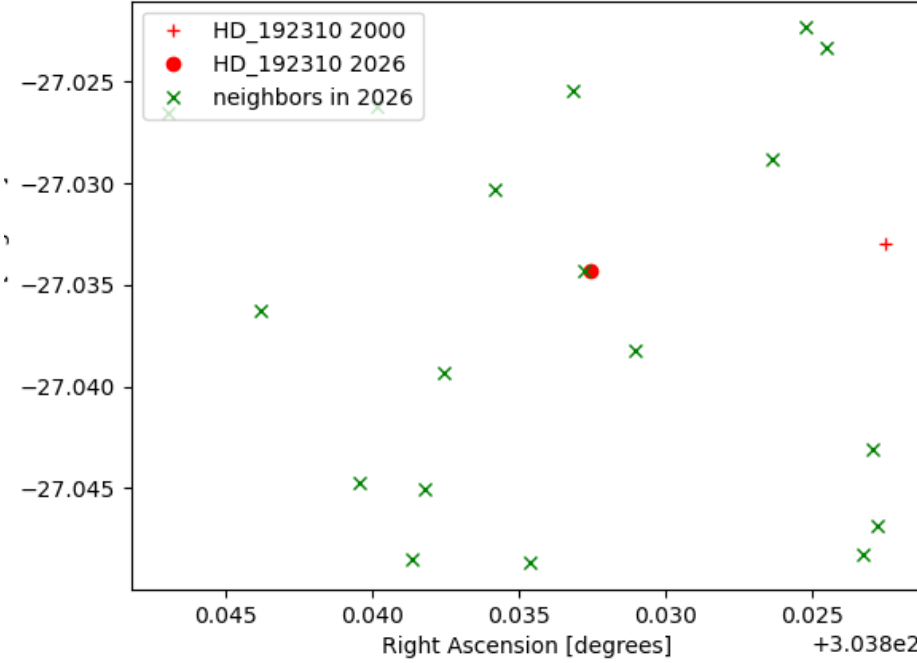


Figure 37. Positions of HD 192310 in 2000 and 2026 compared with positions of other Gaia sources within one arcminute.

Table 20 Positions of stars within one arcminute of HD 192310 in 2026. Target star in bold italics.

Source ID	Distance (arcseconds)	RA	Dec	G mag
6847164651447229824	14.8892	20h15m19.4504s	-27d02m17.5145s	19.2364
6847164647150392448	36.6899	20h15m22.5026s	-27d02m10.5662s	19.3436
6847164651446895488	17.693	20h15m20.5916s	-27d01m49.1442s	18.4647
6847164617088100864	52.2473	20h15m20.3002s	-27d02m55.2518s	16.2898
6847164647150384512	45.4111	20h15m21.7004s	-27d02m41.1497s	19.269
6847164647150384384	42.8784	20h15m21.1715s	-27d02m42.2414s	17.5829
6847164651447693952	24.0703	20h15m21.0043s	-27d02m21.4283s	15.3184
6847164617085484672	58.3593	20h15m17.5844s	-27d02m53.6408s	19.6933
6847164617085486976	44.2277	20h15m17.4997s	-27d02m35.1048s	19.7001
6847164617085485312	55.1083	20h15m17.4624s	-27d02m48.7384s	20.5997
6847164582725738624	54.7861	20h15m21.2752s	-27d02m54.5829s	20.1428
<b>6847167606385195648</b>	<b>0.6338</b>	<b>20h15m19.856s</b>	<b>-27d02m03.5115s</b>	<b>5.4532</b>
6847167602089745280	49.0277	20h15m18.0482s	-27d01m20.4053s	19.3449
6847167606384717952	31.9246	20h15m19.9541s	-27d01m31.5522s	20.9071
6847167606384777472	28.0007	20h15m18.3239s	-27d01m43.663s	20.6226
6847167606382733824	47.0421	20h15m17.8834s	-27d01m24.0365s	18.9931

6847170522665663872	53.9561	20h15m23.2711s	-27d01m35.6403s	17.9361
6847173481897986048	37.3216	20h15m21.5544s	-27d01m34.2786s	20.4011

### A.13 HD 217107

There is no Hubble data for HD 217107, so the analysis only includes the Gaia catalog and Besançon models. The first plot shows the comparison of the Gaia catalog to the Besançon models, showing source counts per square arcminute broken out by Gaia G magnitudes. The second figure and the table show the star positions from Gaia within one arcminute of the target star in 2026.

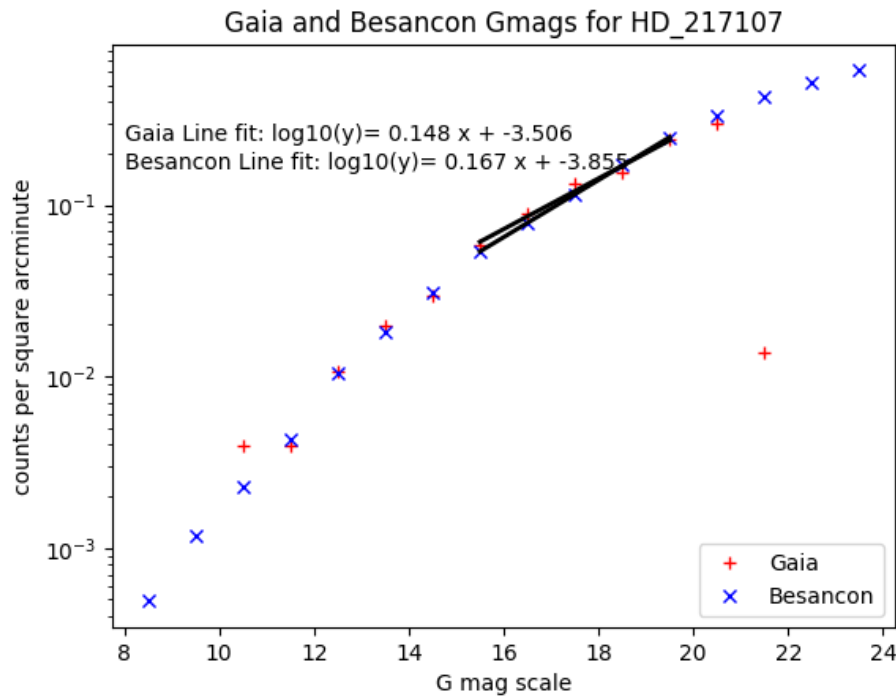


Figure 38 Gaia counts per magnitude bin per square arcminute compared to Besançon simulations of the same for HD 217107.

The position of HD 217107 in 2026 in RA, Dec is 22h58m15.5288s -02d23m43.7682s as calculated from coordinates and proper motions found in SIMBAD in J2000 coordinates.

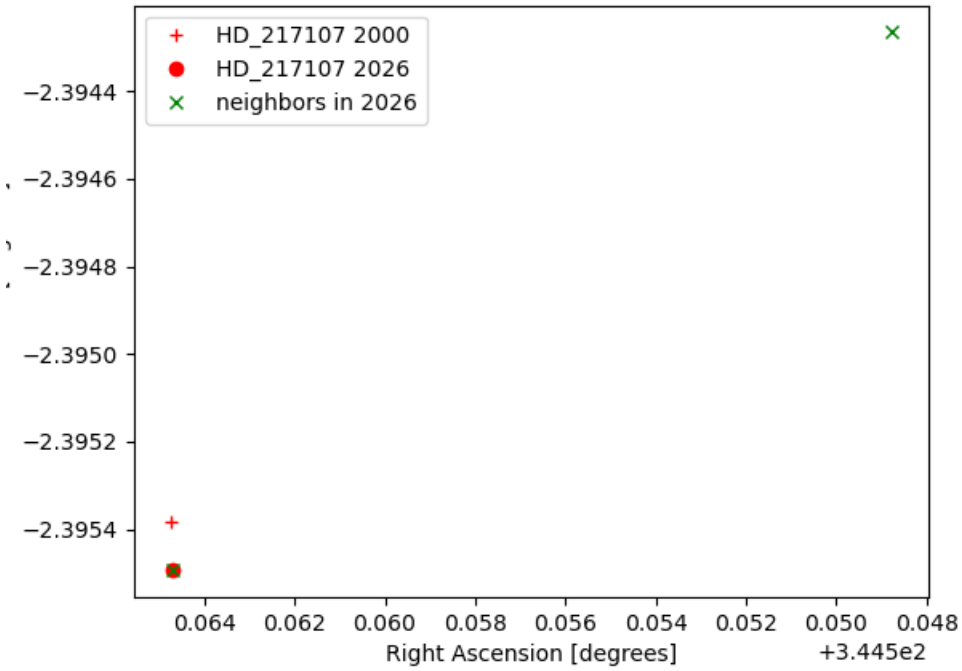


Figure 39 Positions of HD 217107 in 2000 and 2026 compared with positions of other Gaia sources within one arcminute.

Table 21 Positions of stars within one arcminute of HD 217107 in 2026. Target star in bold italics.

Source ID	Distance (arcseconds)	RA	Dec	G mag
2648914005997582848	57.5421	22h58m11.7006s	-02d23m39.3569s	17.1701
<b>2648914040357320576</b>	<b>0.0109</b>	<b>22h58m15.5286s</b>	<b>-02d23m43.7787s</b>	<b>5.9546</b>

### A.14 HD 219134

There is no Hubble data for HD 219134, so the analysis only includes the Gaia catalog and Besançon models. The first plot shows the comparison of the Gaia catalog to the Besançon models, showing source counts per square arcminute broken out by Gaia G magnitudes. The second figure and the table show the star positions from Gaia within one arcminute of the target star in 2026.

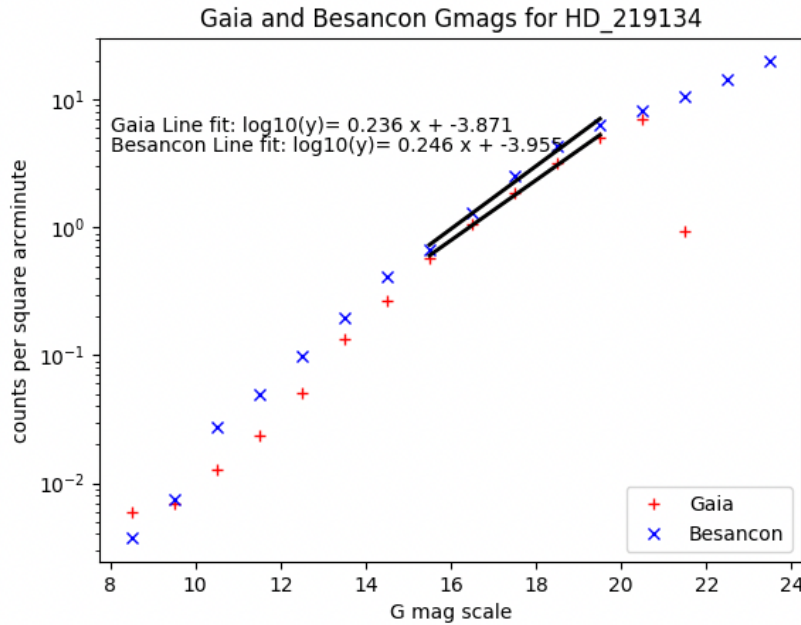


Figure 40 Gaia counts per magnitude bin per square arcminute compared to Besançon simulations of the same for HD 219134.

The position of HD 219134 in 2026 is 23h13m23.6074s +57d10m13.7339s as calculated from coordinates and proper motions found in SIMBAD in J2000 coordinates.

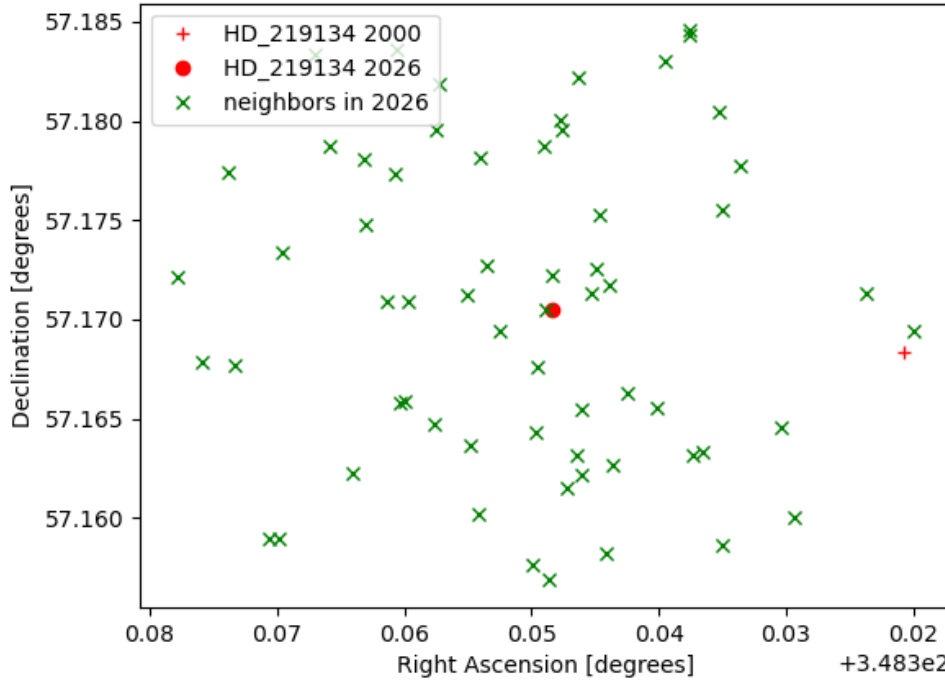


Figure 41 Positions of HD 219134 in 2000 and 2026 compared with positions of other Gaia sources within one arcminute.

Table 22 Positions of stars within one arcminute of HD 219134 in 2026. Target star in bold italic.

Source ID	Distance (arcseconds)	RA	Dec	G mag
2009481027319050496	55.5486	23h13m29.7097s	+57d10m38.7052s	20.7285
200948098666978944	34.2054	23h13m20.9459s	+57d09m47.2485s	18.7406
2009481027319054208	57.8659	23h13m30.6863s	+57d10m19.629s	20.2735
2009480988667022336	32.4368	23h13m23.318s	+57d09m41.3827s	17.8235
2009481027319039616	22.0887	23h13m26.3162s	+57d10m15.371s	20.9173
2009480992961023616	24.0147	23h13m21.6381s	+57d09m55.8395s	18.7241
2009481027319042048	45.3103	23h13m27.8139s	+57d10m43.4516s	20.759
2009480992960630912	10.664	23h13m23.8917s	+57d10m03.3235s	20.5609
2009480958597538432	42.6651	23h13m27.3798s	+57d09m44.0858s	20.2433
2009480992955886720	34.5459	23h13m20.7721s	+57d09m48.0109s	19.0872
2009481023036052480	27.6722	23h13m25.8442s	+57d09m52.8815s	19.0444
2009480954303554560	38.6277	23h13m24.9947s	+57d09m36.7908s	18.4266
2009481023022883840	34.481	23h13m26.5718s	+57d10m38.3897s	18.2558
2009481027315617792	13.3658	23h13m25.2191s	+57d10m16.3541s	19.4456
2009481027317000576	25.337	23h13m26.7184s	+57d10m15.1225s	20.3014
2009480992962046720	6.71491	23h13m22.8597s	+57d10m16.5826s	20.1234

2009481027321303424	12.938	23h13m24.8504s	+57d10m21.8102s	17.5092
2009480924242570496	46.271	23h13m23.9705s	+57d09m27.5573s	18.8524
2009480992962047104	26.6005	23h13m23.1557s	+57d09m47.3884s	17.2669
2009480992962046976	45.0629	23h13m22.5851s	+57d09m29.4448s	17.232
2009480958596176256	59.0218	23h13m28.7722s	+57d09m32.2737s	20.0757
2009480992961024256	41.1881	23h13m19.2794s	+57d09m52.3451s	19.8544
2009481027315635200	28.0649	23h13m26.3919s	+57d09m57.1552s	18.2504
2009480992955893760	49.9194	23h13m20.4083s	+57d09m31.1322s	19.163
2009480992961569664	22.3878	23h13m23.9238s	+57d09m51.4945s	20.3822
2009480992961569024	29.5696	23h13m22.4691s	+57d09m45.651s	16.6586
2009481027321309568	27.6057	23h13m25.1619s	+57d09m49.1934s	17.6908
2009481027321309312	28.7638	23h13m26.4747s	+57d09m56.8939s	19.6326
2009480958596164992	54.5307	23h13m30.2103s	+57d10m04.2343s	19.7227
2009480988672333440	52.9832	23h13m19.0423s	+57d09m35.9365s	17.2657
2009480954312595584	49.691	23h13m29.5906s	+57d10m03.6542s	19.5242
2009480958601837568	59.9895	23h13m28.9465s	+57d09m32.3454s	19.6949
2009480992959292416	30.2805	23h13m23.0685s	+57d09m43.7724s	19.9614
2009481027315609088	32.4989	23h13m27.126s	+57d10m29.1462s	20.3882
2009481027319033600	8.91248	23h13m24.6048s	+57d10m10.0404s	20.4815
2009481027321301888	39.8396	23h13m27.1601s	+57d10m41.1689s	14.0575
2009480924239819008	49.0663	23h13m23.6796s	+57d09m24.6711s	20.632
2009480988667027840	6.31675	23h13m23.6053s	+57d10m20.0506s	14.693
2009480988667001344	19.0875	23h13m22.184s	+57d09m58.5573s	17.5703
2009480992961914752	18.5491	23h13m23.0443s	+57d09m55.7591s	17.3254
2009481027319048448	42.7215	23h13m28.7035s	+57d10m24.1189s	20.5683
2009481778941007104	32.5727	23h13m23.4153s	+57d10m46.2691s	17.3007
2009481783233285504	58.8928	23h13m28.0876s	+57d11m00.0095s	20.7121
2009481783235542656	44.428	23h13m25.7296s	+57d10m54.6741s	19.6712
2009481744577538688	18.6796	23h13m22.7291s	+57d10m30.9941s	16.9988
2009481748876290560	10.1785	23h13m22.7661s	+57d10m21.27s	20.2204
2009481748876290432	9.77799	23h13m22.5298s	+57d10m18.0723s	18.7009
2009481748874726784	55.6533	23h13m16.7793s	+57d10m10.0056s	19.5007
2009481783229836416	29.6363	23h13m23.7679s	+57d10m43.3414s	19.7264
2009481783229834752	52.8477	23h13m26.5538s	+57d11m00.8399s	20.2361
2009481783229839360	37.1854	23h13m25.8134s	+57d10m46.307s	20.6047
2009481748870088704	38.7761	23h13m20.0743s	+57d10m39.7766s	19.834
2009481783233276288	29.806	23h13m24.9578s	+57d10m41.4438s	20.2626
2009481748870094208	48.2292	23h13m17.6873s	+57d10m16.6231s	18.7532

2009481783229832448	34.4227	23h13m23.4597s	+57d10m48.1356s	17.676
<b>2009481748875806976</b>	<b>1.0478</b>	<b>23h13m23.7348s</b>	<b>+57d10m13.8942s</b>	<b>5.2079</b>
2009481817589559936	48.3121	23h13m21.4863s	+57d10m58.8631s	19.4796
2009481748870085376	44.1261	23h13m20.4651s	+57d10m49.7102s	20.0844
2009481817595273600	54.8275	23h13m21.0225s	+57d11m04.3734s	14.3557
2009481783235539840	42.221	23h13m23.13s	+57d10m55.7761s	17.3344
2009481817589551872	54.0687	23h13m21.0219s	+57d11m03.5485s	14.8521
2009481748875803776	31.6585	23h13m20.403s	+57d10m31.7147s	19.1224

### A.15 $\tau$ Ceti

There is Hubble data for  $\tau$  Ceti in MAST, though there are no images of the position in 2026. The closest in the archive is an image from 1997 in the HLA, hst\_06887\_35\_wfpc2\_total\_wf\_drz.fits, in which the 2026 position is just off of the image edge. The position of the target in 2000 is shown in green, while the 2026 position is beyond the image edge and marked in red.

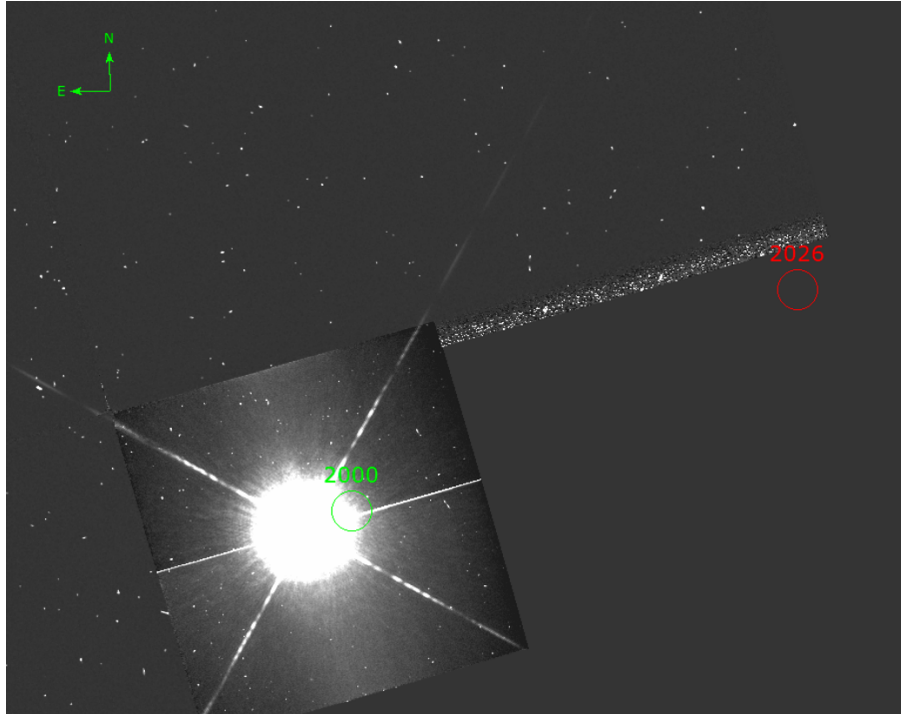


Figure 42 Hubble WFPC2/PC HLA image of  $\tau$  Ceti taken in 1997. The circle in green shows the 2000 position, while the circle in red shows where the star will be in 2026.

There are two parallel fields with WFPC2 in the F606W filter. A visual examination of these fields in the Hubble Legacy archive shows that the fields are almost entirely galaxies or very faint point sources. Some of the sources are spurious (multiple hits on a single galaxy, for instance). Taking the field that allowed us to narrow down the field by the number of images in which the sources were identified, and ensuring that the sources were found in more than one image, there are 67 identified sources.

Table 23 Comparison of total sources in one WFPC2 combined image (total and broken out by CI value) compared to the Gaia catalog for the area around  $\tau$  Ceti.

Catalog being used	Area of coverage (square arcsec)	Total number of sources	Source density per square arcminute
Total of WFPC2	5.7	67	11.8
Sources with $CI < 1.2$	5.7	8	1.4
Sources with $CI > 1.2$	5.7	59	10.4
Gaia (within $r=18$ arcmin)	1017.9	685	0.67
Besançon	360000.0	169120	4.7

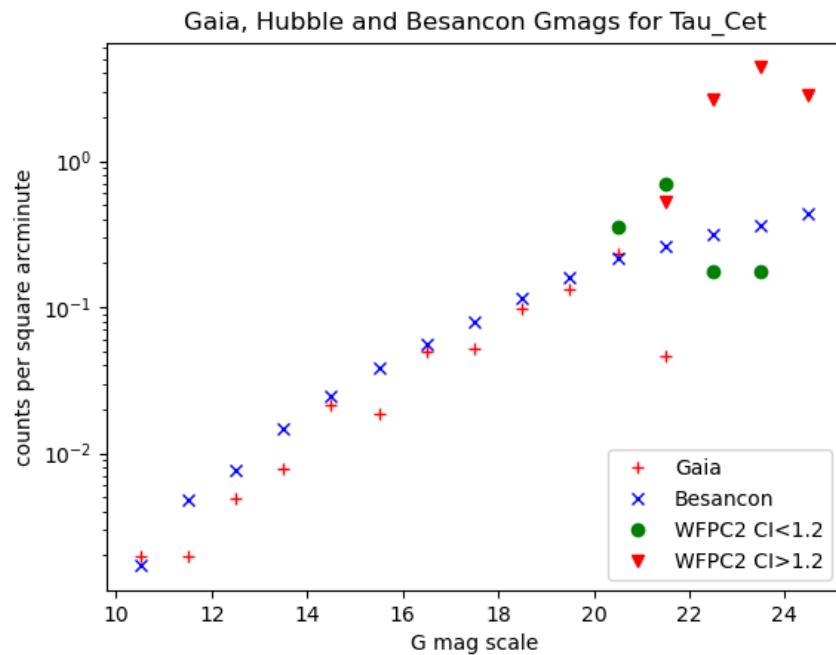


Figure 43 Comparison of Gaia, WFPC2 and Besançon source counts per magnitudes per square arcminute near  $\tau$  Ceti. The WFPC2 data is separated out into point sources ( $CI < 1.2$ ) and extended sources ( $CI \geq 1.2$ ).

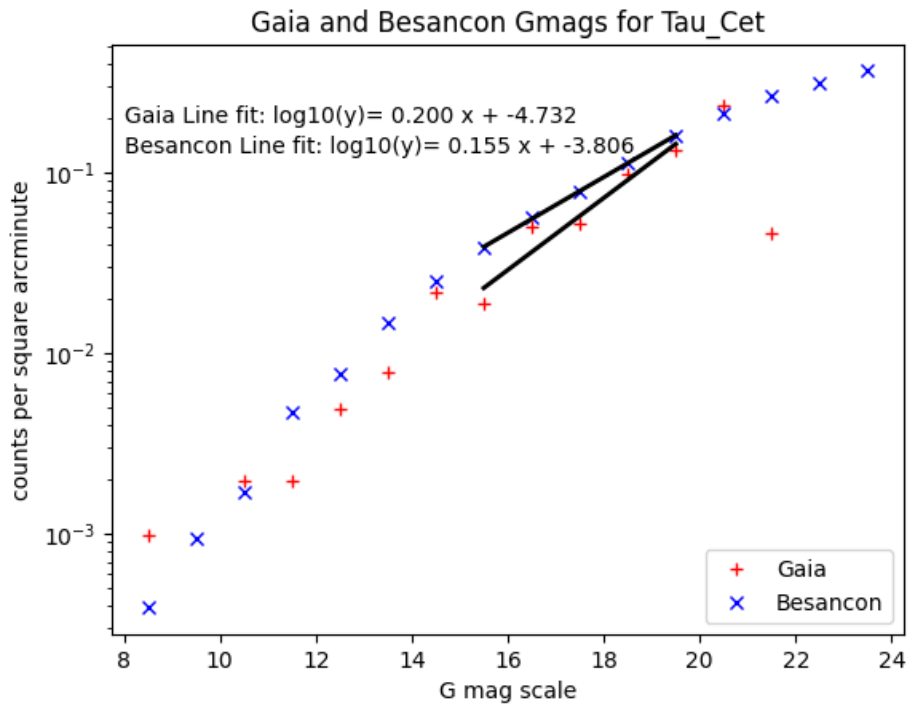


Figure 44 Gaia counts per magnitude bin per square arcminute compared to Besançon simulations of the same for  $\tau$  Ceti.

The position of  $\tau$  Ceti in 2026 is 01h44m00.9811s -15d55m52.7167s as calculated from coordinates and proper motions found in SIMBAD in J2000 coordinates.

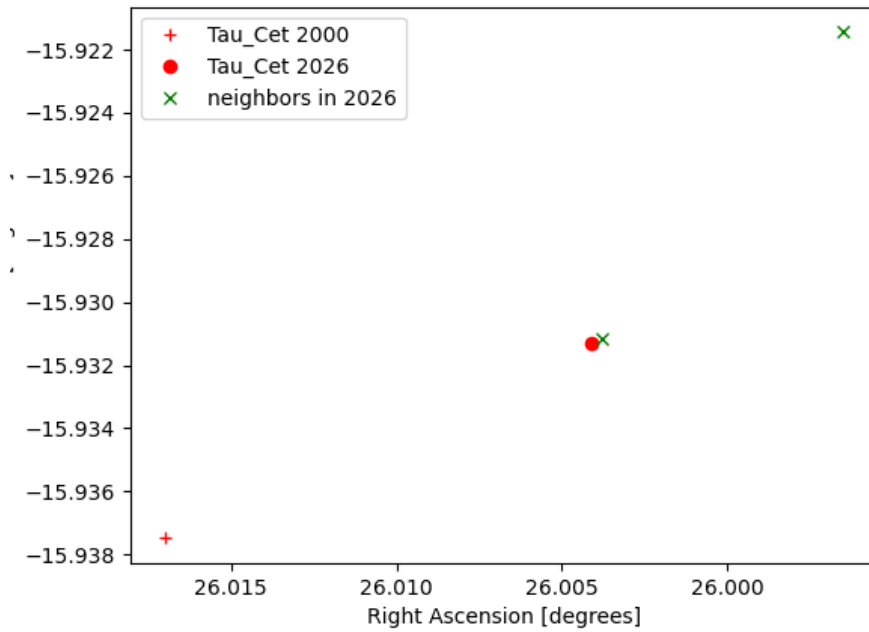


Figure 45 Positions of  $\tau$  Ceti in 2000 and 2026 compared with positions of other Gaia sources within one arcminute.

Table 24 Positions of stars within one arcminute of  $\tau$  Ceti in 2026. Target star in bold italics.

Source ID	Distance (arcseconds)	RA	Dec	G mag
<b>2452378776434276992</b>	<b>1.07258</b>	<b>01h44m00.9136s</b>	<b>-15d55m52.2649s</b>	<b>3.1336</b>
2452379051311170304	44.2041	01h43m59.156s	-15d55m17.2063s	17.7728